PROCEEDINGS A

royalsocietypublishing.org/journal/rspa

Research

Check for updates

Article submitted to journal

Subject Areas:
Geophysics, Geology, Hydrology

Keywords:
Landscape Evolution, Stochastic, Probability, Markov Process, Fluvial, Advection

Author for correspondence:
Gareth Roberts
e-mail: gareth.roberts@imperial.ac.uk

A theory of stochastic fluvial landscape evolution

G. G. Roberts[1,2] and O. Wani[2,3]

[1]Department of Earth Science and Engineering, Imperial College London, London, SW7 2AZ, UK
[2]Division of Geological and Planetary Sciences, California Institute of Technology, Pasadena, CA 91125, USA
[3]Department of Civil and Urban Engineering, New York University, Brooklyn, NY 11201, USA

Geometries of eroding landscapes contain important information about geologic, climatic, biotic and geomorphic processes. They are also characterised by variability, which makes disentangling their origins challenging. Observations and physical models of fluvial processes, which set the pace of erosion on most continents, emphasise complexity and variability. In contrast, the spectral content of longitudinal river profiles and similarity of geometries at scales $\gtrsim 100$ km highlight relatively simple emergent properties. A general challenge then, addressed in this manuscript, is development of a theory of landscape evolution that embraces such scale-dependent insights. We do so by incorporating randomness and probability into a theory of fluvial erosion. First, we explore the use of stochastic differential equations of the Langevin type, and the Fokker-Planck equation, for predicting migration of erosional fronts. Second, analytical approaches incorporating distributions of driving forces, critical thresholds and associated proxies are developed. Finally, a linear programming approach is introduced, that, at its core, treats evolution of longitudinal profiles as a Markovian stochastic problem. The theory is developed essentially from first principles and incorporates physics governing fluvial erosion. We explore predictions of this theory, including the natural growth of discontinuities and scale-dependent evolution, including local complexity and emergent simplicity.

THE ROYAL SOCIETY PUBLISHING

1. Introduction

A characteristic feature of continental landscapes is their variability, see e.g. [1]. Spectral analyses of fluvial geometries, for instance, emphasise considerable scale-dependence [2]. Geomorphic and geologic observations indicate that physical landscape evolution is determined by tectonic, hydraulic and biotic processes operating across a broad range of spatial and temporal scales. The span of scales is many orders of magnitude, i.e. < 1 to $> 10^7$ meters (sediments to continents), and < 1 to 10^7 years. As such, disentangling the origins of landscapes and a general, self-consistent, theory for their evolution remains elusive. Here we explore how information about the natural randomness of processes driving landscape evolution and erosional thresholds can be used to develop such a theory. We use it to investigate scale-dependent evolution of landscapes and their emergent properties.

Erosion by rivers appears to set the pace of landscape evolution in most mid-low latitude continents, see e.g. [1]. It is generally agreed that the geometries of longitudinal river profiles, i.e. elevation as a function of distance, $z(x)$, provide useful information about histories of driving processes, e.g. uplift and erosion. We therefore focus on developing a stochastic theory for the evolution of river profiles. We note that stochasticity has been extensively studied with respect to hillslope evolution, hydrologic processes and especially sediment transport, see e.g. [3–10] and references therein. As far as we are aware, stochasticity has not been used to develop theories of fluvial network evolution at larger scales. Consequently, we address three questions in this paper. First, how can the natural randomness of the forces that drive and resist erosion be incorporated into a theory of fluvial erosion? Secondly, what are the emergent properties of such a theory? Finally, how can observations of erosion and landscape geometries be used to understand the scales at which fluvial landscapes acquire their form when randomness is inherent? We are especially interested in quantifying likely geometries and trajectories of longitudinal river profiles subject to random forcing of erosional processes at scales that are measurable in the field or laboratory.

We explore three approaches to incorporate stochasticity into a theory of fluvial landscape evolution. First, we examine how stochasticity could be incorporated into models of erosional 'front' (e.g. waterfall, knickpoint, knickzone) retreat using equations of Langevin's type. A natural next step is to relate these equations to partial differential equations that can predict the temporal evolution of probability density functions of displacements of erosional fronts (i.e. Fokker-Planck). We briefly examine limitations of using such approaches to understand landscape evolution. Second, we explore the use of semi-analytical approaches that can incorporate distributions of probabilities of erosion to calculate expected displacements of erosional fronts and their variance, by making use of Chapman-Kolmogorov forward equations. Finally, flexible numerical approaches that can incorporate arbitrary geometries and random variables, are used to explore the emergent properties of river profile geometries in the presence of stochastic driving forces and thresholds for erosion. To begin, we summarise relevant existing approaches used to understand how river profiles acquire their geometries.

2. Geometries and evolution of longitudinal river profiles

A broad array of processes, operating at a large range of spatial and temporal scales, contribute to the development of longitudinal river profiles. Evolution of topography at the largest spatial (up to 10^4 km) and temporal scales (up to 100 million years) is largely governed by histories of horizontal and vertical motion of the lithosphere driven by geologic processes (e.g. plate shortening, mantle convection). At these scales, the sedimentary flux histories of continents, recorded by, for example, stratigraphy along passive margins, the longitudinal profiles of

rivers, radiometrically dated histories of fluvial incision and indirect geochemical estimates of denudation (e.g. thermochronometry) attest to the efficacy of erosional processes and the long-term (up to 10^7 years) variability of erosion rates, see e.g. [11–15] and references therein. Observations such as these are used to parameterise phenomenological models of landscape evolution, which are briefly summarised in the following section.

(a) Phenomenological and spectral approaches

The Stream Power model is probably the most widely used approach to predict evolution of longitudinal river profiles, see e.g. [16–20]. It features as an important constituent in landscape evolution models that can, for example, incorporate hillslope erosion, sedimentation, discharge variability, erodibility contrasts and the biosphere, see e.g. [21,22]. Derivations of the Stream Power model often start with postulates such as, erosion rate is a power law function of shear stress, or that erosion rate is a product of shear stress and mean (water) velocity. Sometimes erosional thresholds are explicitly incorporated, and the capacity of a river to transport sediment is considered, see e.g. [19]. The resultant family of models provides kinematic descriptions of river profile evolution. They are parameterised empirically, for example the constants in the power laws are tentatitvely related to lithology, jointing and fracturing, or weathering, say. They can also be calibrated by minismising misfit between for example measured incision rates, or by fitting river profile shapes, see e.g. [23]. A simple version of the Stream Power model, in one dimension, can be expressed by the following partial differential equation

$$\frac{\partial z}{\partial t} = -vA(x)^m \left(\frac{\partial z}{\partial x}\right)^n + U(x,t), \tag{2.1}$$

where A is upstream drainage area, incorporated into the equation of motion as a means to involve increases in water discharge that are often observed downstream. $A(x)$ increases monotonically downstream, with occasional sudden jumps as tributaries join, and can, in some situations, be approximated by x^2 and in some special cases is broadly proportional to x. v, m and n are tuneable parameters that ensure dimensionality. They are calibrated to predict rates at which longitudinal profiles evolve and thence their geometries (and thence, in more general models, landscape evolution). This version of the Stream Power model takes the form of a non-linear advection equation with a source term (uplift rate, U), it is sometimes generalised to include erosional 'diffusivity', which is omitted here for simplicity, see e.g. [16,17,19].

Despite its utility for understanding and predicting landscape form across a variety of space and time scales, a fundamental basis for this, essentially phenomenological, model is lacking. Parameterisation of the Steam Power model, and in fact understanding processes that determine fluvial geometries, typically depends on the scale being studied. As such there is significant disagreement about its validity, and how best to parameterise the model, across scales of interest, see e.g. [20]. In particular, it is challenging to reconcile the predictions of this model with observations of erosion at small scales and physics-based insights into fluvial erosion that emphasise the importance of considering forces, and source terms (e.g. biota), that do not feature in such kinematic models, see e.g. [24]. Hence there is little agreement about how best to generate general insights into landscape evolution using this approach, especially when the basic postulates underpinning the approach may be invalid (e.g. in landscapes dominated by 'glassy' dynamics [25]; continuity is not expected). In that sense, it is challenging to derive (and certainly parameterise) this model from first principles. Nonetheless, we start by exploring how such approaches could incorporate stochasticity. We are especially interested in understanding how complexity at smaller scales might be incorporated and used to assess the probability of the emergent geometries predicted by this family of models. We then move on to consider an entirely different approach to understand the evolution of longitudinal river profiles that does not rely on the assumption of continuity.

One way to incorporate additional complexities (or uncertainties in the underpinning postulates) is via the incorporation of noise, $\eta(x,t)$, such that the Stream Power model becomes

$$\frac{\partial z}{\partial t} = -vA(x)^m \left(\frac{\partial z}{\partial x}\right)^n + U(x,t) + \eta(x,t). \tag{2.2}$$

One reason for taking such an approach arises from spectral analyses of longitudinal river profiles [26,27]. Wavelet transforms of actual river profiles, $z(x) \rightarrow z(x,k)$, where k is wavenumber (spatial frequency), provide information about the power spectral content of profiles, i.e. $\phi(x,k)$, which is helpful for assessing scaling regimes and a guide to the physical processes governing landscape evolution, see e.g. [27] and references therein. Consider that at scales $\gtrsim 100$ km many large river profiles can be broadly characterised by red noise (i.e. they have spectral slopes close to -2; $\phi(k) \propto k^{-2}$). However, at smaller scales (down to ~ 1 km) spectral slopes tend to be ≈ -1 and perhaps 0 (or even 1) at the shortest wavelengths, i.e. pink to white (to perhaps blue) noise characteristics. In contrast, spectral analyses of river profiles extracted from landscape evolution models parameterised using the Stream Power model in the form presented in Equation 2.1, or its two-dimensional equivalent $\partial z_t = -vA^m\nabla^n + U(x,y,t)$, have spectral characteristics that depend on the inserted uplift history, initial conditions and to a far lesser extent the numerical methods used to solve these partial differential equations. These conditions often (for the two-dimensional case) incorporate random noise or flow directions to enforce channelisation. Such models can often reproduce the (e.g. red noise) spectral characteristics at longer (e.g. > 100 km) wavelengths but not exhibit observed spectral 'whitening' at shorter wavelengths [27].

(i) Adding noise by inference and known unknowns

Adding (e.g. quenched) noise to the solutions of these equations, either directly or via an additional source term, are obvious ways to generate more realistic spectral content [27–30]. However, doing so is somewhat arbitrary in that, as of yet, there is no firm independent basis to quantify the contributions (i.e. amplitudes at specific wavenumbers) of various landscape phenomena (e.g. lithological contrasts, biota) to elevations or rates of change of elevation. Consider, for example, lithology or lithological contrasts over which a river flows. An obvious and widely held intuition is that fluvial substrate must be an important determinant of landscape form. For instance, empirical evidence from measured erosion rates of rocks in the laboratory and field shows that 'hard' rocks (more formally, those with high tensile strengths) can be less prone to erosion than 'soft' rocks, see e.g. [30,31]. A corollary is that high elevations in landscapes may be associated with 'hard' rock and changes in relief are associated with changes in rock strength. That intuition is fraught. Consider, for example, that the geometries of the longitudinal profiles of large rivers are almost entirely determined at wavelengths > 100 km, which is typically much greater than the wavelength of lithological change across most landscapes [27]. It is also almost certainly much larger than the rate of jointing and fracturing, which likely play a crucial role in determining substrate erodibility, at Earth's surface, but are (generally) poorly understood [32]. In other words, it is clear that tensile strength of e.g. individual clasts measured in the laboratory, or perhaps at specific localities in the field, can vary considerably, and determine erosion rates at small scales. However, this variability is not manifest in the geometries of river profiles at large scales ($\gtrsim 100$ km), where most of the form of large rivers is determined. In short, it appears that substrate contrasts are unimportant for determining the majority of the form of fluvial landscapes (at large scales).

Even if reliable schemes to convert substrate into erodibility emerge, a fundamental challenge remains—fluvial erosion, by necessity, removes substrate. As such, we have almost no observations (of e.g. joint spacing, lithology, sedimentary cover) that could be used to parameterise models with specific substrate erodibilities for the vast majority of the lifetime of

a river. One way to address this challenge is to explicitly incorporate the natural randomness of erosion into a theory of landscape evolution.

(b) Emergence of simplicity and importance of uplift at large scales

In fact, it is straightforward to use simple versions of the Stream Power model (e.g. Equation 2.1), or its two dimensional equivalent, to generate theoretical profiles that have low residual misfit to actual profiles, i.e. $rms \approx 1$ [14,23,34–36]. For instance, changes in erosion rate due to substrate contrasts, precipitation rate or biota, need not be incorporated. In itself this result is not surprising, nor particularly important, in that many models could fit the data equally well. However, in conjunction with sparse observations of long-term incision rates and the spectral power of river profiles, it provides an indication that, at long wavelengths ($\gtrsim 100$ km), additional erosional complexity is not *required* to fit the available data, i.e. the geometries of observed longitudinal profiles. Moreover, damped inverse models that use Equation 2.1 to predict uplift rate histories yield results that match independent observations of, for example, net uplift constrained by the elevation of (ancient) marine rock, see e.g. [27,36]. These results indicate that families of river profiles, e.g. those draining a particular uplifted region—a domal swell for instance—have common geometries determined by the history of uplift, e.g. [39]. Cross wavelet spectral power of the profiles of families of rivers draining, for example, the Bié dome in Angola yield a consistent view [40]. In short, at wavelengths $\gtrsim 100$ km and on timescales $\gtrsim 1$ Ma observed incision histories of large rivers, the spectral content of river profiles, and very simple advective models of erosion, indicate that erosion need not necessarily be very complicated to generate large-scale geometries of observed river profiles.

(c) Erosional complexity at smaller scales

In contrast, erosional processes and profile geometries at smaller scales are extremely diverse. For example, substrate strength, discharge variability, biota and sedimentation can play important roles in governing local erosion rates and profile shapes [34]. A variety of physics-based models of erosion seek to provide understanding of landscape evolution at spatial and temporal scales up to, say, O(1 km) and O(1 ka). Many models tend to, understandably, focus on erosional processes at scales where experiments are reproducible (e.g. in flume tanks) or at scales in which driving processes can be constrained in the field, see e.g. [24]. For example, physics-based models of block toppling, in which the propensity of a single block (or column) of rock to topple (i.e. erode) derived from simple torque calculations that incorporate body forces, drag form and shear stresses, do a reasonably good job of explaining independent geologic observations of e.g. waterfall retreat rates in some settings at scales O(1–1000 m) and O(1–1000 years), see e.g. [24,33]. There are many other similar examples of physics-based studies that consider, for example, rock plucking, abrasion, sediment transport and landscape evolution in response to viscous creep at similar, relatively small scales, compared to the entire evolving fluvial system; e.g. [25]. Many physics-based approaches emphasise the importance of erosion at the 'atomistic' scale, here O(1 m) or less, once a threshold has been exceeded (e.g. once shear stress is sufficiently high that bed-load particles can be moved or entrained in a flow; drag is sufficiently high to topple rock columns; tensile strength of impacted substrate is exceeded).

This study is principally concerned with understanding whether these scale-dependent views—emergent simplicity and local complexity—of landscape evolution can be reconciled. An obvious challenge emerges, how can diverse and scale-dependent erosional processes be incorporated into a general theory of fluvial erosion? Moreover, how can uncertainties and variability (or randomness) in the forces driving and resisting erosion be absorbed into such a theory?

3. Stochastic migration of erosional fronts

One approach to assess whether erosional processes operating at small scales can lead to the kinematic behaviour predicted by, for instance, the Stream Power model at larger scales, is to compare expected locations of erosional 'fronts' (e.g. knickpoints, waterfalls) and their variance. A simplifying first step is to assume that the velocity, α, at which kinematic waves propagate upstream is constant and deterministic. Hence, when $U = 0$, Equation 2.1 then has the well known characteristic solution $z = z_0(x - \alpha t)$, where $z_0 = z(x, 0)$ is the initial condition. The time taken for an erosional wave to propagate distance L upstream is simply $\tau_G = \int_0^L \mathrm{d}x/\alpha = L/\alpha$, and total distance travelled in time τ_G is $L = \tau_G \alpha$. Similar approaches are central to a variety of techniques used to understand fluvial landscape evolution (e.g. 'χ' analyses; 'Gilbert' times; see e.g. [41,42]).

Exposure ages downstream of the Dettifoss and Selfoss waterfalls in Iceland indicate that such an erosional model, i.e. broadly constant advective velocities (unique for each waterfall), is a reasonable starting point on spatial and temporal scales of O(1 km) and O(1 ka) [37]. However, simple physical models and the variability of measured retreat rates indicate that there is considerable inconsistency in retreat velocities at smaller scales. They likely depend on a variety of space- and time-dependent phenomena include discharge, rock strength and orientation of jointing and fracturing [1]. Consequently, in the following section, these observations are used to explore how stochasticity might be incorporated into such simple models of landscape evolution. This approach could be, for example, used to introducing randomness associated with changes in, say, discharge, lithological contrasts and biota, or to incorporate uncertainties in model parameterisation.

(a) Stochastic waterfall retreat: Equations of Langevin's type

^{3}He exposure ages of fluvial terraces downstream of Dettifoss and Selfoss indicate that the waterfalls are expected to have had positions $x \approx x(0) - vt$ during the last few thousand years, where time, t, is chronological (not geological) time. For Dettifoss $v \approx 0.69$ m /year, and $v \approx 0.11$ m /year for Selfoss [37]. For instance, Dettifoss is expected to have migrated from $x(0) = 2200$ m downstream of the modern waterfall to its current position in ≈ 3200 years (e.g. Figure 1). Stochasticity can be incorporated quite simply by modifying the ordinary differential equation of motion such that

$$\frac{\mathrm{d}x}{\mathrm{d}t} = -v + \sigma\eta(t), \tag{3.1}$$

which has coefficients that do not depend on x. $\eta(t)$ is, say, random white noise. Note that the expected value of $\langle\eta(t)\rangle = 0$ since any non-zero mean can be absorbed into the definition of v. Solutions to this equation can be approximated via the Euler-Maruyama method, in which the equation is first recast as $\mathrm{d}x = -v\mathrm{d}t + \sigma\mathrm{d}W$, where W indicates the Wiener process, and thus x_t is approximated recursively over the (discrete) times of interest by

$$x_{t+\Delta t} \approx x_t - v\Delta t + \sigma\mathrm{d}W_t. \tag{3.2}$$

where $\mathrm{d}W_t$ are independently and identically (i.i.d.) distributed normal random variables, with expected value zero and variance Δt (standard deviation = $\sqrt{\Delta t}$), $\mathrm{d}W \sim \mathcal{N}(0, \sqrt{\Delta t})$. This notation is used to represent normal distributions throughout this paper unless otherwise indicated.

Solutions to this equation are compared to positions of Dettifoss and Selfoss as a function of time estimated from measured exposure ages downstream in Figure 1. For the pathways shown, $\Delta t = 1$ year, $\sigma = 8$ and 2 for Dettifoss and Selfoss, respectively. $v = 0.11$ m /year for Selfoss and $v = 0.69$ m /year for Dettifoss, consistent with the retreat rates estimated by simple linear regression of exposure ages as a function of distance from the waterfalls. 1000 'waterfall' trajectories in distance-time space, calculated using Equation 3.2, are shown by the

overlapping grey curves in Figure 1. The translucent histograms show examples of distributions of displacement at three times. Single realisations, to demonstrate the complexity of individual paths, are shown by the thin black curves. Expected values are simply $\langle x(t)\rangle = \langle x(0)\rangle - vt$ and are shown by the thick white lines in Figure 1. These results demonstrate how stochasticity can be incorporated into simple models of landscape evolution. If σ is too large there are many theoretical trajectories that are not consistent with measured exposure ages, which indicates that such data provide constraints on the distribution of stochasticity in eroding systems.

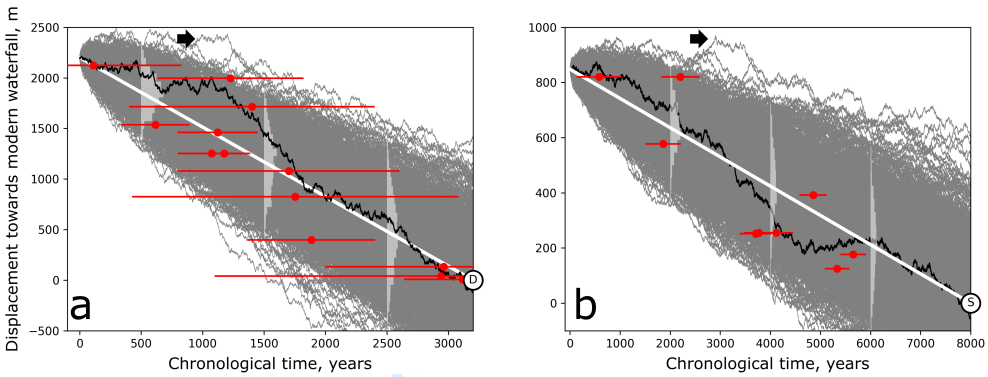

Figure 1. Calculated stochastic retreat of Icelandic waterfalls. (a) Red circles and error bars are calculated using ^{3}He cosmogenic exposure ages of fluvial terraces downstream of Dettifoss waterfall, its modern position is indicated by white circle annotated D, see body text [37]. Grey curves = 1000 solutions to Equation (3.2); white histograms = distribution of displacements at $t = 500$, 1500 and 2500 years. Black curve = single realisation to demonstrate the stochastic trajectory of an individual migrating waterfall. White curve = expected values. (b) Results for Selfoss. Arrows point to examples of trajectories that advance significantly downstream.

(b) Stochastic erosional front migration with rates that depend on location

Most macroscopic models of fluvial erosion assume that erosional fronts migrate upstream with a velocity that depends on location, e.g. retreat rates decrease towards the head of the river (e.g. first term on right-hand side of Equation 2.1). A Langevin-type equation that allows displacement to be a function of position is

$$\frac{\mathrm{d}x}{\mathrm{d}t} = -vx + \sigma\eta(t), \tag{3.3}$$

which has the form of an Ornstein-Uhlenbeck process, see e.g. [43]. Without noise this equation is equivalent to assuming slopes in the Stream Power model (Equation 2.1) retreat with a velocity $\mathrm{d}x/\mathrm{d}t = -vx$ (for $n = 1$). Solutions to the Langevin equation can again be approximated via the Euler-Maruyama method, in which the equation is first recast as $\mathrm{d}x = -vx\mathrm{d}t + \sigma\mathrm{d}W$, which leads to

$$x_{t+\Delta t} \approx x_t - vx_t\Delta t + \sigma\mathrm{d}W_t, \tag{3.4}$$

again $\mathrm{d}W_t \sim \mathcal{N}(0, \sqrt{\Delta t})$. For a deterministic value of x_0 (i.e. the initial value of x at time, $t = 0$), $\mathrm{Var}(x_0) = 0$, and expected values (of x_t) for a Ornstein-Uhlenbeck process are straightforward to calculate by integrating the deterministic part of Equation 3.3

$$\langle x_t|x_0\rangle = \langle x_0\rangle \exp(-vt). \tag{3.5}$$

where $|$ is the probabilistic notation for 'given'. Variance, calculated by rearranging Equation (4.4.29) in [2], is

$$\mathrm{Var}(x_t) = \frac{\sigma^2}{2v}\left[1 - \exp(-2vt)\right], \tag{3.6}$$

and standard deviation $= \sqrt{\mathrm{Var}(x_t)}$. Examples of solutions to Equations 3.4-3.6 are shown in Figure 2. Each pathway (black and grey curves) could be regarded as a possible trajectory of an erosional front, say, a single knickpoint along a river, or an escarpment, in time-distance space. In this example, $0 \leq t \leq 3200$, $\Delta t = 1$, $\sigma = 5$ and $v = 5 \times 10^{-4}$. The front starts at $x_0 = 2200$ (dimensions of length) and propagates head-ward (towards lower x_t). The propagation velocity depends on the distribution of noise, the value of the tuneable parameter v, as well as position, x, such that erosional velocities (on average) decrease head-ward. They demonstrate that even in the presence of noise that generates complex pathways for single erosional fronts in time-distance space, expected (mean) values and variance follow smooth trajectories. These trajectories can be calculated analytically for specific distributions of noise.

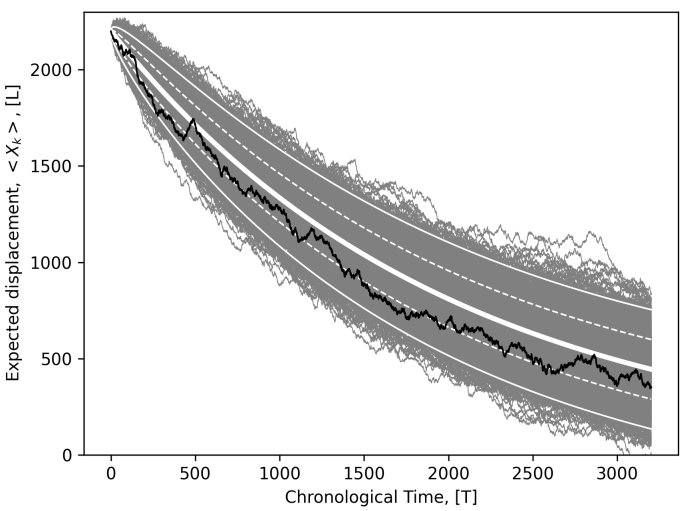

Figure 2. Solutions of stochastic differential equation to estimate retreat pathways of erosional fronts when velocity decreases upstream. Grey curves = 1000 solutions to Equation (3.4); black curve = 1 realisation demonstrating an individual path. Thick white curve = expected values calculated using Equation 3.5. Thin dashed and solid white curves = $\sqrt{\mathrm{Var}(x_t)}$ and $2\sqrt{\mathrm{Var}(x_t)}$, respectively (see Equation 3.6).

(c) Stochastic erosional front migration with the Fokker-Planck equation

Equations of Langevin's type are readily related to equations that calculate the temporal evolution of the probability density function of the system. Here, the stochastic migration of an erosional front upstream developed in the previous section is described in terms of a probability density function, $P(x,t)$. The probability of finding an erosional 'front', e.g. waterfall, knickzone, at position (state) x is specified at time t. The Ornstein-Uhlenbeck Equation 3.4 can be expressed as the Fokker-Planck (sometimes called Kolmogorov's) equation. Trajectories of Ornstein-Uhlenbeck processes can be described by,

$$\frac{\partial P(x,t)}{\partial t} = v\frac{\partial}{\partial x}\left[xP(x,t)\right] + \kappa\frac{\partial^2 P(x,t)}{\partial x^2}, \tag{3.7}$$

where $\kappa = \sigma^2/2$. A reasonable starting condition is $P(x|t=t_0) = \delta(x - x_0)$, such that the probability density of an erosional front is assumed to take the form of a Dirac-delta distribution centred at x_0 at time t_0. The probability density of the erosional front (which must integrate to 1)

can then propagate and spread from x_0. A way to think about this scheme is that the advective (drift) part of this equation (first term on right-hand side) is related to the deterministic part of the Langevin equation (see Equation 3.4), and the diffusive part (second term on right-hand side) describes the spread of variance (see histograms in Figure 1). We note that such an approach has already been used to develop stochastic theories of sediment transport, e.g. [11].

Following [44], solutions to Equation 3.7 are found by performing a Fourier transform with respect to x. In the frequency domain where the probability distribution is given by $\tilde{P}(k,t)$,

$$\frac{\partial \tilde{P}}{\partial t} = -vk\frac{\partial}{\partial k}\tilde{P} - \kappa k^2 \tilde{P}, \tag{3.8}$$

where k is wavenumber; $\partial/\partial x \to ik$ and $x \to i\partial/\partial k$. This equation can be solved via the method of characteristics. The Fourier transform of the probability density, from the wavenumber to the spatial domain, is

$$P(x,t|x_0,t_0) = \frac{1}{2\pi}\int \exp(-ikx)\tilde{P}(k,t|x_0,t_0)\mathrm{d}k. \tag{3.9}$$

Given the assumed (δ distribution) starting condition, the initial condition, in the wavenumber domain, is $\tilde{P}(k,t_0|x_0,t_0) = \exp(-ikx_0)$. The solution to Equation 3.8, making use of the method of characteristics, is thus

$$\tilde{P}(k,t|x_0,t_0) = \exp\left\{-ikx_0\exp\left[-v(t-t_0)\right] - \kappa k^2\left(1-\exp\left[-2v(t-t_0)\right]/(2v)\right\}. \tag{3.10}$$

By inserting this equation into Equation 3.8, integrating, and performing the Fourier transform, the following solution is obtained,

$$P(x,t|x_0,t_0) = \left(\frac{v}{2\pi\kappa\left\{1-\exp\left[-2v(t-t_0)\right]\right\}}\right)^{1/2}\exp\left\{-\frac{v(x-\exp(-v(t-t_0)x_0)^2}{2\kappa\left[1-\exp(-2v(t-t_0))\right]}\right\}, \tag{3.11}$$

which takes the form of a Gaussian distribution that can be regarded as the Green's function for this problem. Figure 3 shows solutions to this equation compared to solutions to the Langevin equation (Equations 3.5–3.6). In this example, $\sigma = 1$, $v = 0.01$, $x_0 = 100$. As [44] points out, solutions to Equation 3.11 become the stationary distribution, indicated by the dashed line in Figure 3, when $v(t-t_0) \gg 1$.

These complimentary approaches provide means to incorporate stochasticity into theoretical approaches to understand how erosional fronts propagate upstream. However, a problem with tackling landscape evolution problems in this way is that large advances (i.e. waterfalls propagating downstream), although rare, are permitted. As an example consider the single paths, indicated by arrows in Figure 2, that advance downstream for significant portions of their history. Whilst small advances may be physically realistic, large advances are almost certainly not. In other words, the probabilities of erosion used to parameterise stochastic models of fluvial erosion need more careful consideration, and probably a more flexible framework, for assessing how stochasticity impacts landscape evolution, which is the focus of the remainder of this paper.

4. Self-consistent theory of scale-dependent landscape evolution

The approaches explored so far have assumed that probabilities of erosion have well-defined distributions, which may not always be the case in reality. They are also somewhat removed from the actual physical processes governing landscape evolution at small scales. Consequently, we now explore how probabilities of erosion at small scale can be estimated and used to explore landscape evolution across the scales of interest. For instance, we seek to understand whether local erosional process are likely to combine in such a way that such behaviour emerges naturally. We are principally concerned with understanding whether parsimonious, probabilistic models of fluvial erosion, derived from first principles, or as near as reasonable, are consistent with the

royalsocietypublishing.org/journal/rspa Proc R Soc A 0000000

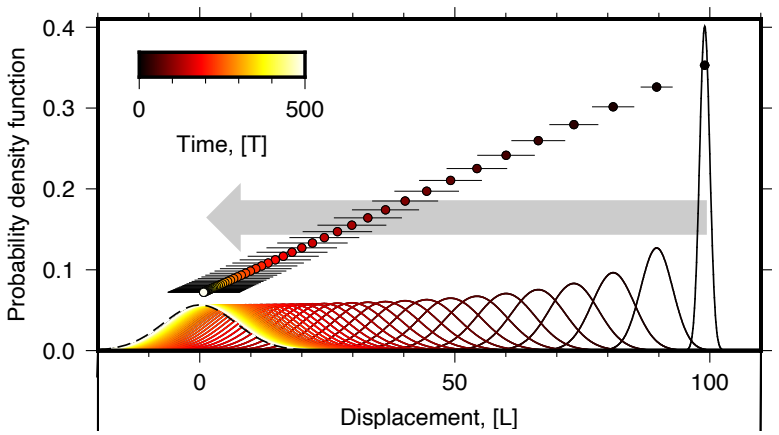

Figure 3. Solutions of Fokker-Planck differential equation for retreat pathways of erosional fronts when velocity decreases upstream. Coloured lines = solutions to Fokker-Planck equation at times t (see Equation 3.11). Dashed curve = stationary solution to Fokker-Planck equation: $P_{st}(x) = \sqrt{v/2\pi\kappa}\exp\left[-vx^2/2\kappa\right]$. Expected values from solutions to the equivalent to Langevin equation and standard deviation, $\sqrt{\mathrm{Var}(X_s)}$, are shown by coloured circles and error bars (see Equations 3.5–3.6). Note that position of circles on ordinate are staggered for clarify.

emergent behaviour observed in nature and predicted by widely used phenomenological models.

(a) Markovian evolution of river profile geometries

Most physical models of erosion, at their core, are simply a statement that material will be removed once a threshold has been exceeded. Consequently, we start by exploring the emergent properties of a very simple Markovian model of erosion such that

$$z_{t+1}^{x} = \begin{cases} z_t^x & \text{if} \quad F \leq c^* \\ z_t^x - \delta_z & \text{if} \quad F > c^* \end{cases} \tag{4.1}$$

where z is elevation above a datum (e.g. the equipotential surface), x and t indicate location and time with indices $\{0, 1 \ldots N\}$, respectively (see Figure 4). δ_z is (vertical) erosion and F and c^* are respective applied forces and critical values (thresholds) that must be overcome for erosion to take place. The following, even simpler, formulation of Equation 4.1 produces 'river' profiles that, for specific distributions of F and c^*, mimic solutions to the Stream Power model (Equation 2.1; i.e. propagating kinematic waves) at large length and time scales

$$z_{t+1}^{x} = \begin{cases} z_t^x & \text{if} \quad \Delta z \leq c \\ z_t^{x-1} & \text{if} \quad \Delta z > c \end{cases} \tag{4.2}$$

where $\Delta z = z_t^x - z_t^{x-1}$. Location $x-1$ is downstream of x. During a single time step of this model (of length δ_t), either erosion (i.e. elevation reduction, Δz) occurs such that an erosional 'front' (e.g. a waterfall; knickpoint) migrates upstream by one hop (of length δ_x), or erosion does not occur. In this deterministic model, erosion occurs when a change in relief, Δz, exceeds a critical value, c. In fact, $\Delta z > c$ could be regarded as any situation in which erosion occurs when a threshold is exceeded (for many conceivable models of erosion; [45]).

This evolution equation is an initial value problem in which the dynamics of the system, $z(x,t)$, are determined *a priori* by the starting condition i.e. $z(x,0)$ and the value(s) of c. The process appears to be irreversible such that recovering z_{t-1}^x from (only) z_t^x is not obviously tractable.

In fact, it appears that this problem is not even tractable if we know locations at which erosion occurred (from $t-1 \rightarrow t$) and the value of c; consider that any $\Delta z > c$ will result in erosion and hence z^x_{t-1} could have any value, such that $z^x_{t-1} - z^{x-1}_{t-1} > c$. This inference implies that predicting historic river profile shapes using deterministic physics-based models such as this one is likely to be fraught.

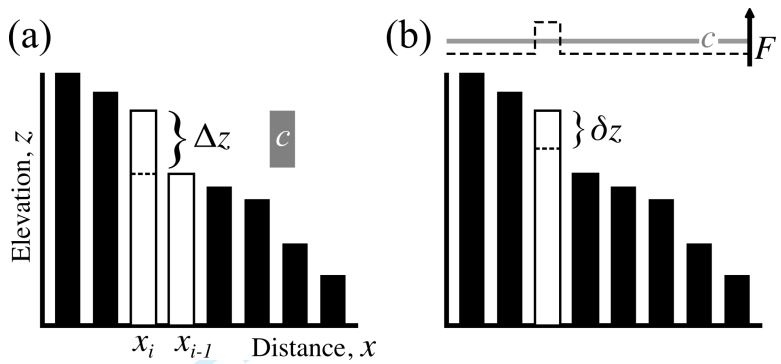

Figure 4. Two Markovian erosional schemes for longitudinal river profile evolution. (a) Erosion occurs only if $\Delta z > c$, where Δz = relief between adjacent 'blocks' (separated here for clarify; i.e. $z_i - z_{i-1}$, where z is elevation), and c = threshold for erosion, indicated here by height of annotated grey bar. Distance (e.g. along a river; x) has discrete spatial indices i. Note that in this example only the blocks labeled x_{i-1} and x_i are active between time steps t and $t + \delta_t$ such that block x_i is eroded (reduced in elevation) by Δz to the elevation of block x_{i-1} (dashed line), in other words Δz is migrated upstream by δ_x. (b) A more flexible scheme in which erosion, δz, occurs if forces exceed critical thresholds; black dashed and solid grey lines labelled F and c, respectively.

(i) Data availability

Measurements of river profile elevations through time are sparse globally, similarly we do not usually know specific histories of thresholds for erosion. Perhaps the most complete set of observations that constrain the evolution of a longitudinal profile on long time scales arise from K-Ar dating of ~ 23 Ma incised basaltic flows in South Eastern Australia, see e.g. [15]. In contrast, measurements of modern elevations (and hence Δz) exist for nearly all rivers. Modern river profile geometries can be mapped at resolutions down to O(10 m) using satellite technologies (e.g. Copernicus, TanDEM-X). At specific localities high resolution digital elevation models have been generated and can used to assess landscape change on timescales up to centuries (e.g. from repeat laser or photogrammetric surveying) but they tend to be sparse and at small scales, e.g. [37]. Assessing changes in relief for most rivers, by comparing recent and older global digital elevation models is perhaps possible (e.g. Shuttle Radar Topographic Mission, 2000-2014, [46]). However, given the longevity and resolution of existing global digital elevation models, quantifying local changes in erosion from these datasets likely requires erosion rates to be O(1–10 m/year), which is extremely high and hence unlikely to yield representative insight into landscape evolution across the scales of interest. From a geologic (longer term) perspective, the specific values of these functions are likely to always be extremely difficult to determine. Consider, for example, that discharge, which is used to calculate e.g. drag, depends on precipitation rate, and we only have records that extend, at most, a few decades to hundreds of years.

However, if we assume that modern parameters (e.g. Δz; critical thresholds) are representative of erosional systems more generally, determining probabilities that erosion occurs and associated statistical moments (e.g. expected value, variance) is tractable. In the subsequent sections we

describe and apply a probabilistic approach to understand emergent behaviour for specific distributions of, say, F, Δz or c. More formally, we seek to address the question, what is the impact of $P(\Delta z > c)$, and similarly $P(F > c)$, on the emergent behaviour of the system described by Equations 4.1 and 4.2? It is trivial to show by brute force computation that, at large scales, such models can yield profiles that are similar to those predicted by the Stream Power model for similar starting conditions, see e.g. [1,17,19,23]. An obvious extension is to allow F, z (or Δz), and c to be random variables and explore their impact on the evolution of the erosional system using, say, a Monte Carlo style approach. However, we first explore whether any analytical insight can be gained by considering Δz and c as probability distributions.

(b) Erosional probabilities in a Markovian model

As a first step, consider the transition probabilities for the simple Markovian problem described above (see Figure 4). Consider an erosional front (e.g. a knickpoint or a waterfall) moving incrementally along a river (along the x axis). The front can either jump to the left with step δ_x (with probability p) or stay where it is (with probability $1-p$) at each time step s, which could be regarded as a Poisson process. Time $\tau = s\delta_t$, where δ_t is the length of the time step (e.g. hours, days, years, decades). In this simple model erosion is treated as a one-sided, one-step, random walk. If a jump occurs, cell elevation is reduced to the elevation of the cell downstream as per Equation 4.2. We discuss more general models later. In terms of transition probabilities

$$P(x_i \to x_{i-1}, t \to t+\delta_t) = p, \quad \text{(eroding)} \tag{4.3}$$

$$P(x_i \to x_i, t \to t+\delta_t) = 1-p, \quad \text{(static)}. \tag{4.4}$$

It would be useful to know the probability of finding elevation z at position x at time $t+\delta_t$ given these probabilities of stasis and erosion. Consequently, the transition probability equations are recast, such that the Master equation is

$$P(x, t+\delta_t) = (1-p)P(x,t) + pP(x-\delta_x, t) \tag{4.5}$$

where P indicates the probability distribution of elevation, z, as a function of space and time. Since we are considering time steps that are very small (e.g. seconds to years) compared to the overall evolution of a landscape (e.g. hundreds of thousands to tens of millions of years) we perform a Taylor expansion, such that in the continuum limit

$$P(x,t) + \delta_t \frac{\partial P(x,t)}{\partial t} + O(\delta_t^2) = (1-p)P(x,t) + p\left[P(x,t) - \alpha\delta_t \frac{\partial P(x,t)}{\partial x}\right] + O(\delta_x^2). \tag{4.6}$$

Noting that $\delta_x = \delta_t \alpha$, where α is the 'transition velocity' (i.e. jump rate), which could be estimated using, for example, the toppling rate of eroding blocks. Ignoring the second order terms and higher,

$$\frac{\partial P(x,t)}{\partial t} \approx -\alpha p \frac{\partial P(x,t)}{\partial x}. \tag{4.7}$$

When $p = 1$ this formulation is similar to a version of the macroscopic advective Stream Power erosional model (e.g. Equation 2.1 without uplift) with constant advection velocity (with units of e.g. 1 m /year for the block toppling example given above).

(c) Stochastic displacement of individual erosional fronts

Alternatively, and perhaps more intuitively, the evolution model could be recast to calculate the expected position of a migrating erosional front (i.e. $x_{i-1} \to x_i$) during time step δ_t. In turn we could estimate emergent advection velocities or sum them to yield expected travel times of erosional fronts, or distances moved. We could, for instance, calculate the probability that N erosional 'events' occur within a given time by drawing samples from a binomial distribution.

These values could then be used to calculate the expected distance an erosional front will have travelled and its variance. In this simple model, probabilities of 'success' (i.e. erosion occurring) are specified by the probability that a critical threshold for erosion will be exceeded (i.e. p).

First consider the simple case in which the probability, p, of an erosional event during each time step is constant. The probability of N erosional events (hence N head-ward steps of an erosional front) within a given number of time steps, $s = 0, 1, 2 \ldots n$, can then be calculated using the binomial probability mass function

$$P(N) = \binom{s}{N} p^N (1-p)^{s-N}, \tag{4.8}$$

where the number of combinations of erosional events in s time steps is given by the binomial coefficient $\binom{s}{N} = s!/N!(s-N)!$. For instance, if the total number of time steps in the scenario being considered $s = n = 100$, and the probability that erosion occurs at each time step is independent and a constant $p = 0.5$, the probability that $N \equiv 50$ erosional events will have taken place (and hence the erosional front will have migrated $N\delta_x$ distance upstream) is a maximum $P(50) \approx 0.08$. The probability of erosion decreases with a binomial distribution such that the probability of ($N \equiv$) 20 or 80 erosional events having occurred is $< 10^{-9}$.

(i) Expected retreat distances: single step

In general $p = p(x, t)$, consequently, building on work presented by [11], a more general approach is explored as follows. First, consider the distance travelled by an erosional front at each time step, which is here expressed as Δx_s ($= \delta_x$ if $p = 1$). The expected distance of travel of a single erosional front, $\langle \Delta x_s \rangle$, per time step, incorporating probabilities of motion and stasis, can then be expressed as

$$\langle \Delta x_s \rangle = p\delta_x - [(1-p) \times 0]. \tag{4.9}$$

Note that $(1-p) \times 0$ is the static situation and included for completeness. The second central moment of Δx_s (i.e. variance of the migration distance of the erosional front) for an individual step is given by $\langle \Delta x_i^2 \rangle - \langle \Delta x_i \rangle^2$, such that $\mathrm{Var}(\Delta x_s) = \delta_x^2 p - \langle \Delta x_i \rangle^2 = \delta_x^2 p - (\delta_x p)^2 = \delta_x^2 (p - p^2)$. In other words, this problem takes the form of a Bernoulli trial.

(ii) Expected displacement after s steps

The distance travelled after s time steps is thus $X_s = \sum_{i=0}^{s} \Delta x_s$. The expected total displacement of the erosional front at time $\tau = s\delta_t$ is therefore

$$\langle X_s \rangle = \sum_{i=0}^{s} \langle x_s \rangle = \sum_{i=0}^{s} p_i \delta x \tag{4.10}$$

If p is a constant this equation simplifies to

$$\langle X_s \rangle = sp\delta_x = \frac{\tau}{\delta_t} p \delta_x. \tag{4.11}$$

If the jumps are random independent events (we are treating them as such), then the variance of the total distance traveled (i.e. in time τ) equals the sum of the variances of each random event in the chain of events up to τ. Variance of the total distance moved by the erosional front at time

step s is

$$\mathrm{Var}(X_s) = \sum_{i=0}^{s} \langle \Delta x_i^2 \rangle - \langle \Delta x_i \rangle^2 = \delta_x^2 \sum_{i=0}^{s} p_i - p_i^2 \tag{4.12}$$

and standard deviation = $\sqrt{\mathrm{Var}(X_s)}$. For constant p,

$$\mathrm{Var}(X_s) = \delta_x^2 (p - p^2) s = \delta_x^2 (p - p^2) \frac{\tau}{\delta_t}. \tag{4.13}$$

These equations indicate that for a given probability (p) that erosion occurs within a specific interval of time (δ_t) the variance of possible positions of erosional fronts increases as they propagate upstream. We start by exploring how different probabilities of erosion impact evolution of fluvial systems. To begin with we make four simplifying assumptions. First, the probability of erosion, p, along a river is constant. Second, δ_t and δ_x are unity. Third, relief is normally distributed and, fourth, a constant threshold for erosion, c, exists.

(iii) Expected displacement when $\Delta z \sim \mathcal{N}(\mu_{\Delta z}, \sigma_{\Delta z})$ and c is a constant

Here we are interested in quantifying the probability of erosion, i.e. $p = P(\Delta z > c)$, for different (normal) distributions of Δz defined by mean and standard deviation, $\mu_{\Delta z}$ and $\sigma_{\Delta z}$, respectively. Note that variance is σ^2. In this case, the probability of erosion is simply

$$P(\Delta z > c) = 1 - \Phi\left(\frac{c - \mu_{\Delta z}}{\sigma_{\Delta z}}\right), \tag{4.14}$$

where Φ is the normal cumulative distribution function. Figure 5 shows calculated probabilities for different normal distributions of Δz and values of c. Note that negative and positive Δz are permitted, i.e. river profiles, $z(x)$, do not necessarily need to be monotonic to be incorporated into this approach. In scenarios where $\mu_{\Delta z}$ is much greater than c, $P(\Delta z > c) \to 1$ (i.e. erosion is much more likely; e.g. white triangle in Figure 5b). Conversely, when $\mu_{\Delta z} \ll c$, $P(\Delta z > c) \to 0$ (i.e. stasis is increasingly likely; e.g. black triangle in Figure 5c). Armed with such probabilities it is trivial to calculate the expected distance an erosional 'front' will retreat and its variance through time. For example, if $\delta_x = 1$, $s = 100$, $\Delta z \sim \mathcal{N}(50, 50)$ and $c = 50$, such that $p = 0.5$ (e.g. grey circle in Figure 5b), a front is expected to have migrated $\langle X_s \rangle$ = 50 steps (out of a possible 100) and associated variance $\mathrm{Var}(X_s) = 25$ (Equations 4.11 and 4.13).

(iv) Expected displacement for normal distributions of Δz and c

There are good reasons not to consider c as being normally distributed, simply because $c < 0$ has no obvious physical meaning. Nonetheless, for completeness, consider a simple example in which $\Delta z \sim \mathcal{N}(\mu_{\Delta z}, \sigma_{\Delta z})$ and $c \sim \mathcal{N}(\mu_c, \sigma_c)$. It is then straightforward, because we are working with two normal distributions, to calculate the expected value and variance of $\zeta = \Delta z - c$, they are simply $\mu_\zeta = \mu_{\Delta z} - \mu_c$ and $\mathrm{Var}(\zeta) = \sigma_\zeta^2 = \sigma_{\Delta z}^2 + \sigma_c^2$, respectively. It is then also straightforward to calculate the probability of erosion at each position along a river, $p = P(\Delta z > c)$, such that

$$P(\Delta z > c) = 1 - \Phi\left(0 - \frac{\mu_\zeta}{\sigma_\zeta}\right). \tag{4.15}$$

Appendix A gives a more detailed derivation of Equation 4.15. This approach is sufficiently flexible that the impact of changing the (normal) distributions of Δz and c can be assessed. We will first consider a simple scenario in which $\mu_{\Delta z} = \mu_c$ and $\sigma_{\Delta z} = \sigma_c$, in other words relief and critical values for erosion are assumed to have the same (normal) distributions. In this case, $P(\Delta z > c) = 0.5$ everywhere. Similar to the examples given previously for constant c, in scenarios where $\mu_{\Delta z}$ is much greater than μ_c, $P(\Delta z > c) \to 1$ (i.e. erosion is much more likely). Conversely, when $\mu_{\Delta z} \ll \mu_c$, $P(\Delta z > c) \to 0$ (i.e. stasis is increasingly likely). However, given the challenges associated with interpreting $c < 0$ we do not explore this approach further. Instead we investigate the consequences of incorporating more realistic distributions of Δz into the calculations of probabilities of erosion.

royalsocietypublishing.org/journal/rspa Proc R Soc A 0000000

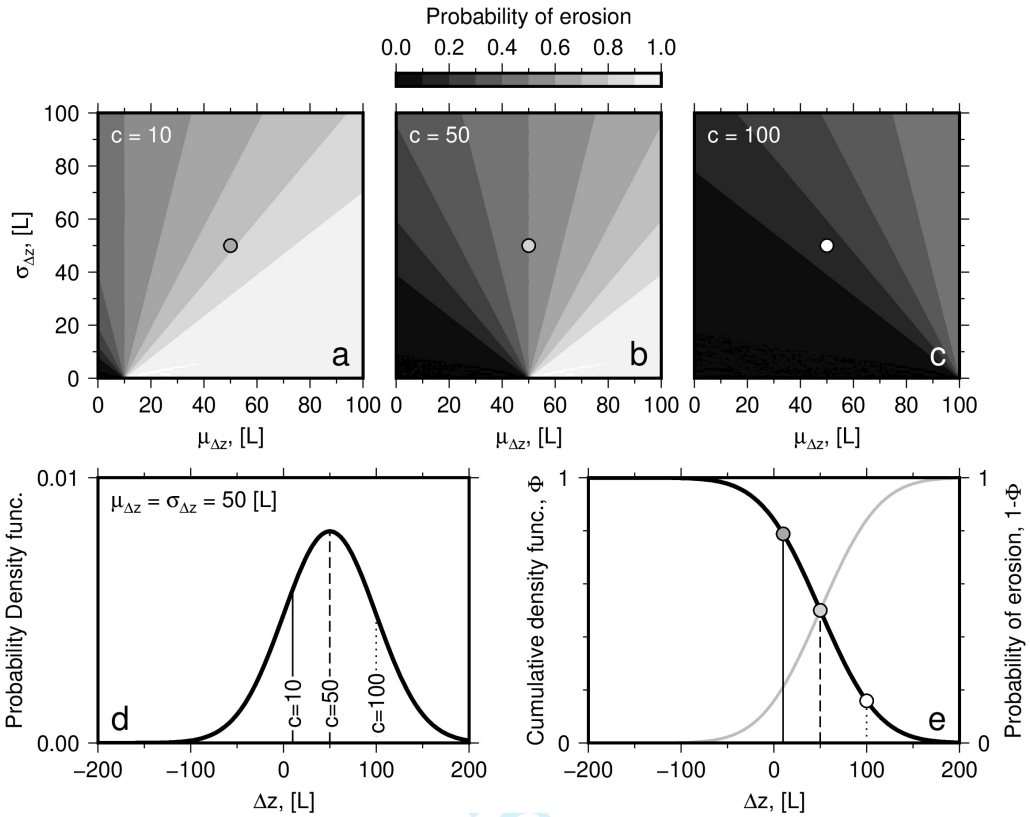

Figure 5. Probabilities of erosion for normal distributions of relief. (a) Grey scale = probability that $\Delta z > c$ (i.e. that erosion occurs) when $\Delta z \sim \mathcal{N}(\mu_{\Delta z}, \sigma_{\Delta z})$, i.e. Δz is assumed to be normally distributed with mean $\mu_{\Delta z}$ and standard deviation $\sigma_{\Delta z}$, and the critical value for erosion is constant ($c = 10$ in this example). White circle indicates locality where $\mu_{\Delta z} = \sigma_{\Delta z} = 50$ (see probability and cumulative density functions in panels (d) and (e), respectively). (b-c) Calculated probabilities for $c = 50$ and 100, all other parameters are held constant between panels (a-c). (d) Thick black curve = example of a probability density function; here $\Delta z \sim \mathcal{N}(50, 50)$. Labelled solid, dashed and dotted lines = values of erosional threshold, c, used to calculate probabilities of erosion at locations indicated by the circles in panels (a-c). (e) Grey curve = cumulative density function, $\Phi(z)$, of Δz. Black curve = $1 - \Phi$, which was used to calculate probabilities that $\Delta z > c$ shown in panels (a-c). Vertical lines and shaded circles correspond to lines and coloured circles in panels (a-d).

(v) Expected displacement for exponential distribution of Δz

One way to quantify the distribution of (global) fluvial relief is to use inventories of waterfall height measurements. Figure 6a shows waterfall heights from `worldwaterfalldatabase.com`, which appears to be the most comprehensive inventory of waterfall heights currently available. We note that waterfall heights are currently being mapped globally (see Hydrosheds: `www.hydrosheds.org`), which could provide additional constraints for the following analyses. The primary benefit of using waterfalls to estimate the distribution of local relief, compared to using digital elevation models (DEMs), is that relief measurements are not necessarily limited by DEM resolution. The particular inventory used in this study does not contain information about relief for waterfalls where $\Delta z < 152$ m or < 97 m (overall relief or highest individual drop). Nonetheless, these data suggest that the probability of local relief in real rivers is broadly exponentially distributed. Consequently, we now consider the probability of erosion when, the

royalsocietypublishing.org/journal/rspa Proc R Soc A 0000000

probability density distribution, $P(\Delta z) \sim \mathrm{Exp}(\lambda)$, such that

$$P(\Delta z) = \begin{cases} \lambda \exp(-\lambda \Delta z) & \text{if} \quad \Delta z \geq 0 \\ 0 & \text{if} \quad \Delta z < 0 \end{cases} \tag{4.16}$$

where λ is the 'rate parameter' ensuring that $\int_0^\infty P(\Delta z) \mathrm{d}\Delta z = 1$. Expected values and variance are $\langle \Delta z \rangle = 1/\lambda$, and $\mathrm{Var}(\Delta z) = 1/\lambda^2$, respectively. An obvious challenge is to define an appropriate value for λ using the available data. The available data are truncated such that we neither known the number of height measurements less than the cutoff, τ^*, say, 150 m for this dataset, nor their values. Hence, the value of λ is estimated using the Maximum Likelihood Estimator, $\mathcal{L}$, for a left-truncated exponential distribution,

$$\mathcal{L}(\lambda | \Delta z_1 \text{ and } \Delta z_2 \ldots \Delta z_n, \tau^*) = \mathcal{L}(\lambda | \Delta z_1, \tau^*) \mathcal{L}(\lambda | \Delta z_2, \tau^*) \ldots \mathcal{L}(\lambda | \Delta z_n, \tau^*) \tag{4.17}$$

$$= \lambda^n \exp\left[\lambda \left(n\tau^* - \sum_{i=1}^{n} \Delta z_i \right)\right], \tag{4.18}$$

where $\Delta z_1, \ldots, \Delta z_n$ are measured waterfall heights within the truncated domain $\Delta z > \tau^*$. The maximum of $\mathcal{L}(\lambda)$ is expected to be where $d\mathcal{L}/d\lambda = 0$, which can be straightforwardly confirmed by plotting the Log-likelihood. Hence, following differentiation of the right-hand side of Equation 4.18, and some simplifications (see Appendix B), we find

$$\frac{1}{\lambda} = -\tau^* + \frac{1}{n} \sum_{i=1}^{n} \Delta z_i = \overline{\Delta z} - \tau^*. \tag{4.19}$$

where $\overline{\Delta z}$ is the mean of the truncated dataset. There are $n = 805$ waterfalls in the inventory with measurements of total overall relief. The cumulative relief of this dataset, truncated at $\tau^* = 150$ m, is 2.6×10^5 m (with mean = 320 m), which indicates $\lambda \approx 6 \times 10^{-3}$ /m. The accuracy of this parameter might be improved if, say, more information about waterfall heights globally becomes available. This distribution is shown by the thick black curve in in Figure 6b, alongside examples where λ increased or decreased by a factor of 2.

It is now straightforward to calculate the probability that erosion will occur for an exponential distribution of Δz if a single, constant, threshold for erosion, c, is assumed,

$$P(\Delta z > c) = \int_c^\infty \lambda \exp(-\lambda \Delta z) \mathrm{d}\Delta z = \exp(-\lambda c), \tag{4.20}$$

noting lower bound on the integral $= c$. If, for example, we assume that $\lambda = 6 \times 10^{-3}$ /m, and $c = 10$ m, then the probability of erosion is 0.94. If $c = 100$ m, $P(\Delta z > c) = 0.55$. Figure 6b shows examples of calculated probabilities of erosion for different values of λ and c. As expected, they demonstrate that increasing rate parameter λ decreases the probability of erosion for a constant critical threshold for erosion. Figure 6d maps probabilities of erosion as a function of the rate parameter and critical erosional threshold. This figure demonstrates the trade-off between the rate parameter and threshold, i.e. erosion is similarly probably for different combinations of λ and c. Inserting a probability of erosion of 0.55 into Equations 4.10 and 4.13, and assuming that $\delta_x = 1$ and $s = 100$, yields an expected total horizontal displacement $\langle X_s \rangle$ = 55 out of a possible 100 steps, with variance 24.75. A central theme in this study is assessment of how variance evolves as erosional fronts migrate upstream.

(d) Head-ward decreases in the probability of erosion

So far we have considered simple scenarios in which the probability of erosion has the same distribution at each locality along a river (e.g. normal with identical means and standard deviations; exponential with same rate parameter value). We now consider more realistic scenarios in which the probability of erosion decreases towards the head of a river. Such scenarios

royalsocietypublishing.org/journal/rspa Proc R Soc A 0000000

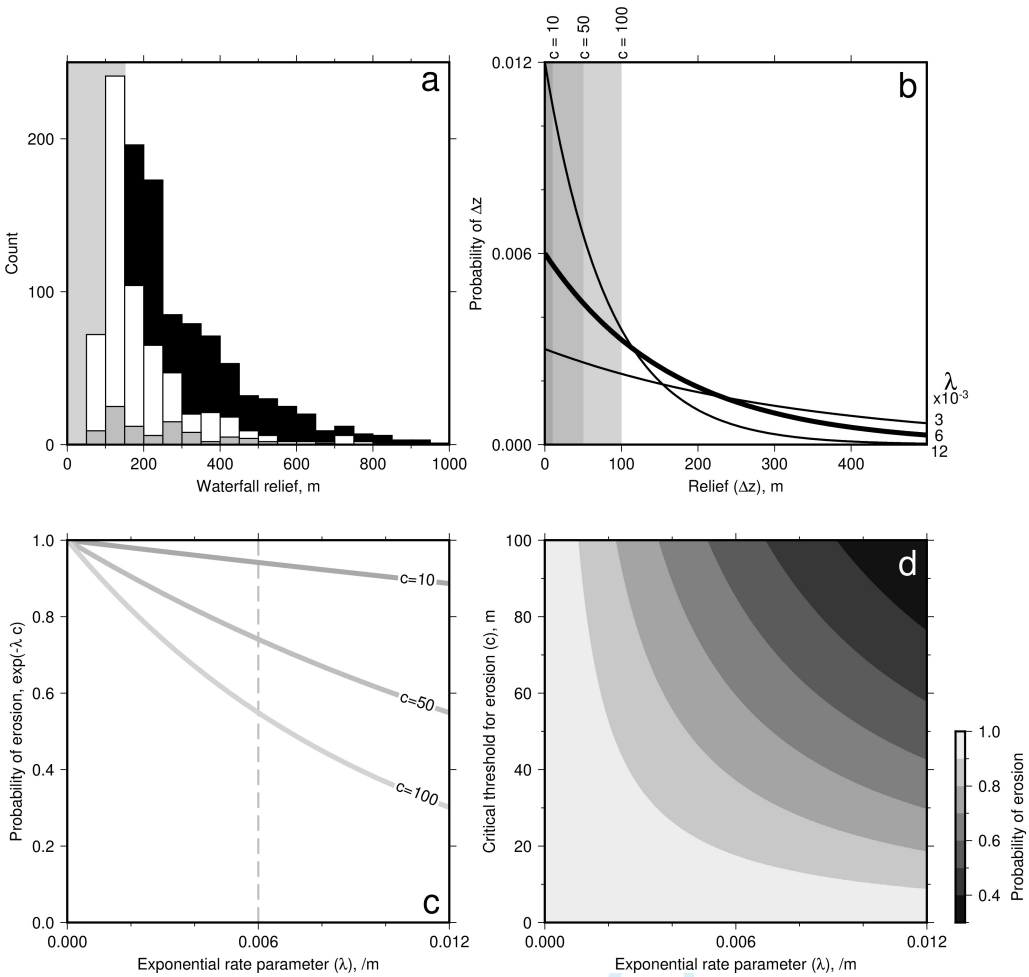

Figure 6. Probabilities of erosion for exponential distributions of relief. (a) Black histogram = number of global waterfalls by overall relief ($n = 805$); data truncated at 152 m (grey rectangle). White = waterfalls by tallest individual drop (truncated at 97 m; $n = 619$). Grey = waterfalls by free falling drop (truncated at 97 m; $n = 90$). (b) Probabilities of relief. Thick black curve = exponential distribution, $\mathrm{Exp}(\lambda)$, with rate parameter, $\lambda = 6 \times 10^{-3}$, calculated using Maximum Likelihood Estimator for the left-truncated distribution of waterfalls (overall relief) shown by black histogram in panel (a). Thin black curves: $\Delta z \sim \mathrm{Exp}(2\lambda)$ and $\mathrm{Exp}(\lambda/2)$. Examples of assumed critical thresholds for erosion, c, are annotated atop the panel, and indicated by grey bands. (c) Probability of erosion as a function of rate parameter, λ, i.e. $P(\Delta z > c|\lambda) = \exp(-\lambda c)$, see body text. Dashed vertical line indicates rate parameter constrained by relief of waterfalls (panel a). Annotated grey curves = probabilities of erosion for annotated critical thresholds. (d) Probability of erosion as a function of rate parameter and critical thresholds for erosion.

might be expected where discharge, and hence power available for erosion, tends to increase downstream.

To start we consider solutions to Equations 4.10 and 4.12 for probabilities of erosion that vary simply as a function of distance along a river (and hence time). For simplicity, temporal and spatial steps are both set to unity, and $s = \tau = 100$. Figure 7 shows results for four scenarios. In the first simple example, we calculate the limits of expected displacements in which probability of erosion p is constant and equal to one (see black lines in Figure 7). This example has expected value $\langle X_s \rangle = s\delta_x$, and variance $\mathrm{Var}(X_s) = 0$ (i.e. this scheme is deterministic). The purple curves

in Figure 7 show results for a scenario in which the probability of erosion for individual time steps decreases linearly upstream. Unsurprisingly, expected displacements are less than when $p(x) = 1$, and variance increases with time; $\langle X_s \rangle = -t^2/4l + t$, where l, here 10^{-2}, is a scaling parameter. Decreasing probabilities of erosion, shown by the red and pink curves, forces expected displacements of migrating erosional fronts to 'plateau', i.e. reach, or tend to, finite expected displacements.

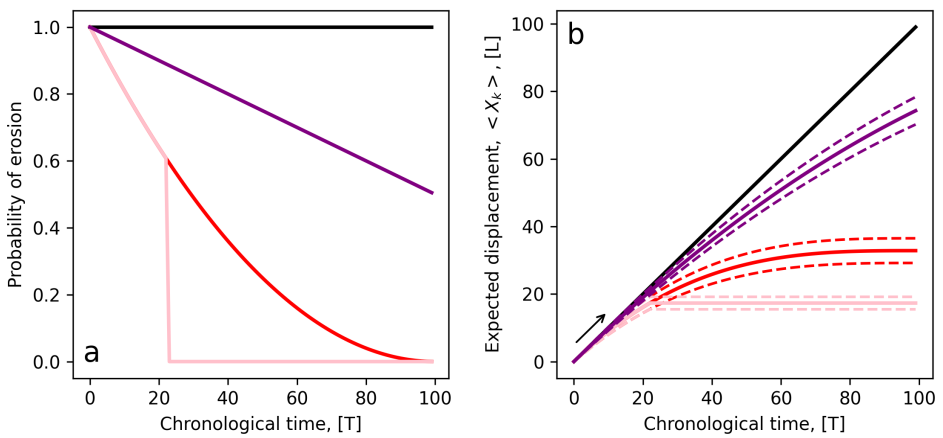

Figure 7. Space-dependent probabilities of erosion. (a) Probabilities of erosion used to generate trajectories of erosional fronts shown in panel (b). (b) Black line = expected displacement (in direction of arrow) of an erosional front for constant probability of erosion ($p = 1$); Equations 4.11 & 4.13. Purple solid and dashed curves = expected displacement and standard deviation, $\sqrt{\mathrm{Var}(X_s)}$ when $p(x) = 1 - xl/2$; Equations 4.10 & 4.12. Red solid and dashed curves: $p = (1 - xl)^2$, respectively; pink solid and dashed curves: $p = (1 - xl)^2$ for $p \geq 0.6$ otherwise $p = 0$; $l = 10^{-2}$.

It is now straightforward to estimate displacements from probabilities of erosion determined by the distribution of forces and critical thresholds, which could vary as a function of space and time. We start by considering the distributions $\Delta z \sim \mathcal{N}$, as proxies for forces available for erosion, explored already. To begin with we explore the simple scenario in which $\Delta z(x) \sim \mathcal{N}(\mu_{\delta z}(x), \sigma_{\Delta z})$, where $\mu_{\delta z}(x) = 1 - xs/2$. In other words we assume that the means of the normal distributions of Δz decrease head-ward and standard deviations are constant. We start by assuming that the critical threshold for erosion, c is constant and identical (Figure 8). We again assume space and time steps are unity, and that $s = \tau = 100$. Higher critical thresholds for erosion reduce probabilities of erosion, and hence expected displacements of erosional fronts for a given time. Second, we explore the implications of assuming that the critical threshold for erosion c is also normally distributed. Figure 4.15 shows results for a scenario in which $c \sim \mathcal{N}(10, 2)$. Expected values and variances are compared to the case in which c is constant and identical (every other parameter value is consistent between the two models). The results indicate that when the critical threshold for erosion is a random variable we should still expect convergence to expected displacement. They provide analytical benchmarks with which we test more general approaches developed in the rest of this paper.

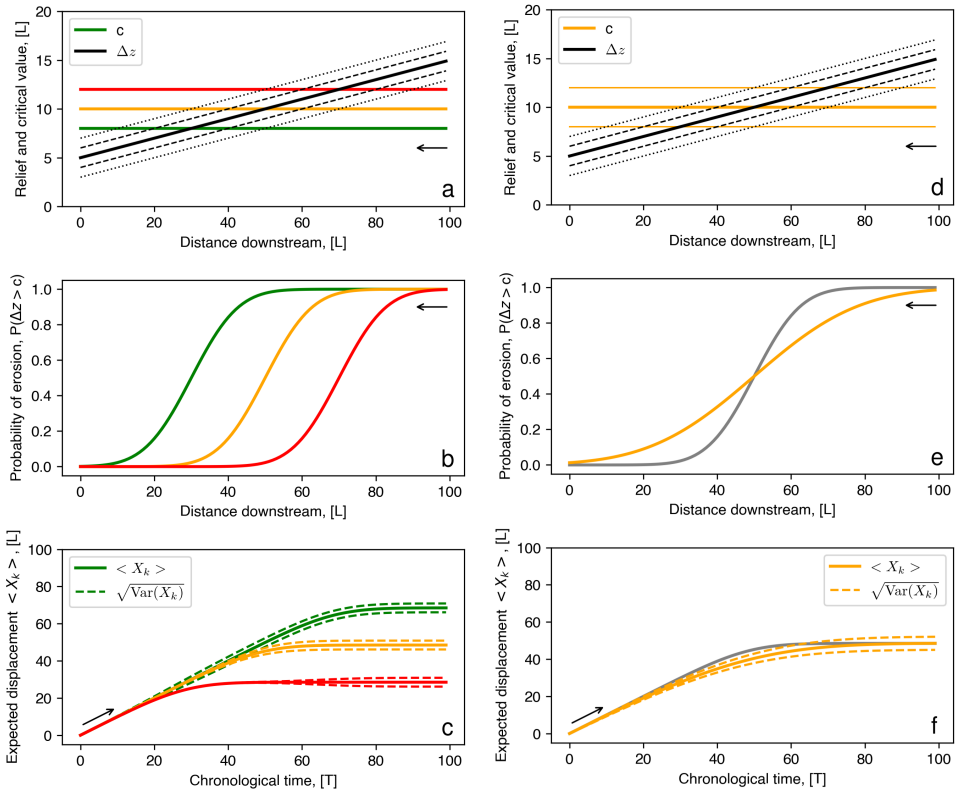

Figure 8. Expected displacements for space-dependent probabilities of erosion incorporating $\Delta z \sim \mathcal{N}$. (a-c) Results for constant critical thresholds for erosion, c. (a) Local relief, Δz, is assumed to be normally distributed with mean indicated by black line; dashed and dotted lines = one ($\sigma_{\Delta z} = 1$) and two standard deviations. Coloured lines = assumed thresholds for erosion. (b) Calculated probabilities of erosion, $P(\Delta z > c)$, as function of distance for critical thresholds indicated in panel a; see Equation 4.14. (c) Expected displacements, $\langle X_s \rangle$, and standard deviations, $\sqrt{\mathrm{Var}(X_s)}$, for three scenarios indicated in panels a-b, see Equations 4.10 and 4.12. Arrows indicate direction of travel of erosional front. (d-f) Probabilities of erosion and expected displacement when $\Delta z \sim \mathcal{N}$ and $c \sim \mathcal{N}$. Orange curves show results for $c \sim \mathcal{N}(10, 2)$ (panel d; Equation 4.15). Grey curves show, for comparison, probability of erosion and expected displacement when $c = 10$ (i.e. orange curves in panels a-c).

(e) Time step length and probabilities of erosion

We might have observations that can provide estimates of probabilities of erosion during specific intervals of time. For instance, we might know the probability that a column of rock will topple once per decade is $p_d = 0.1$. The probability of erosion not occurring during the decade is $1 - p_d$. We might wish to know the probability of erosion at different time scales, for example when parameterising stochastic models of erosion. If we assume that erosional events are independent, the probability of erosion during s time steps is $p_s = 1 - (1 - p_d)^s$, i.e. we simply incorporate all of the probabilities that erosion will not occur during s time steps. For instance, for the example above, the probability of erosion in a century ($s = 10$), is ≈ 0.65. It is straightforward to calculate probabilities of erosion at shorter time scales, such that $p_y = 1 - (1 - p_d)^{1/s}$. For example, the probability of erosion per year, for this simple example, is $p_y \approx 0.0105$ (where, again, $s = 10$). In general, $p_{\delta_t} = 1 - (1 - p_{tc})^{\delta_t / \delta_{tc}}$, where δ_{tc} and δ_t, are respective time step lengths at which

royalsocietypublishing.org/journal/rspa Proc R Soc A 0000000

probabilities of erosion are known or sought, and p_{tc} is the calibrated (observed) probability of an erosional event during time step δ_{tc}.

(f) A stochastic theory of longitudinal river profile evolution

We now return to the development of a stochastic theory of river profile evolution. In general, the distributions of forces available for erosion (or proxies, e.g. Δz) and critical erosional thresholds (c), and hence probabilities of erosion (p) are not necessarily well-behaved functions amenable to analytical attack. Therefore a more general, computational, approach is now explored. In this generalisation, which takes the form of a set of Bernoulli trials that approximate a Poisson process, arbitrary distributions of $F(x,t)$, $\Delta z(x,t)$ and $c(x,t)$, are used to define probabilities of erosion. They are then used to predict the evolution of river profiles, the geometries of which can be compared to expected displacements of erosional fronts and their variance, and, ultimately, real profiles.

The approach adopted is a simple linear programming problem in which, at a single locality along a river, the probability of erosion is drawn from a Bernoulli distribution in which the probability of success (i.e. erosion occurs) is determined by p. A successful draw from the binomial distribution yields a value of 1, and hence the river erodes locally and the erosional front steps head-ward by δ_x. Of course in this problem, many erosional fronts can be stepped head-ward in the same time step. By performing many of these simple calculations, in a Monte Carlo style approach, it is straightforward to investigate emergent behaviours for different probability distributions of forces. We seek to understand whether these numerical approaches, that incorporate reasonable river profile geometries, produce results consistent with analytical (and semi-analytical) approaches described in previous sections to calculated expected displacements and variances of erosional fronts.

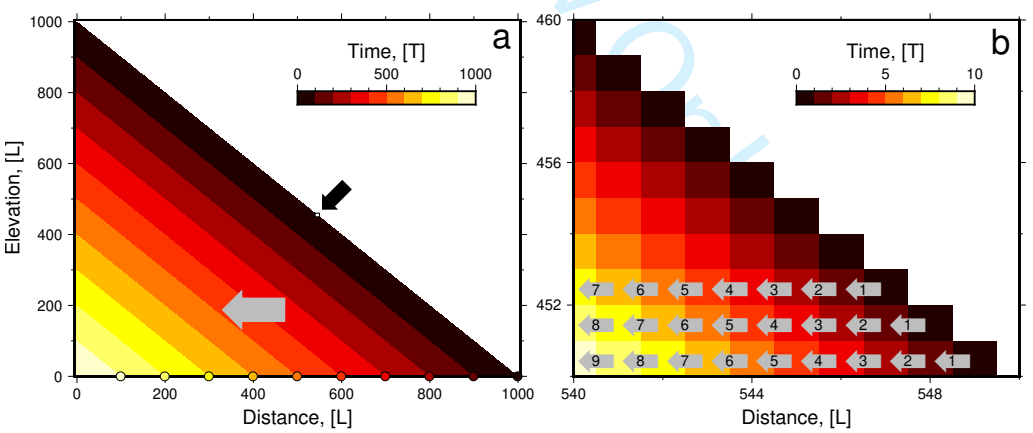

Figure 9. Longitudinal profile evolution when probability of erosion = 1. (a) Colors = longitudinal profiles as a function of time; grey arrow indicates retreat direction. Small white square indicated by black arrow = location of panel (b). Colored circles on x-axis = expected displacement of erosional front starting at (1000,0) calculated analytically using Equation 4.11. Note that variance in this example is zero. (b) Evolution of select individual blocks for first ten time steps. In this simple example, elevations of individual blocks are reduced to the elevation of the nearest downstream block in each time step, e.g. labeled grey arrows for three lowermost rows.

(i) A simple deterministic example

We start with a simple demonstration of the approach using a model in which the probability of erosion $p = 1$ (i.e. $\Delta z > c$, or $F > c^*$, everywhere; Figure 9). The evolution of the longitudinal profile, calculated using Equation 4.2, is compared to expected displacements (circles) calculated using Equation 4.10. Note that in this deterministic experiment variance is zero. Figure 9b shows a 'zoom' into the results for the first ten time steps of this model (within the small white square indicated by the black arrow in panel a). The grey labeled arrows indicate the head-ward stepping of 'blocks' during each time step for lowermost three rows; all rows evolve in a similar way. We now explore the consequences of stochastic driving forces.

(ii) Erosional forces as Ornstein-Uhlenbeck distributions

The Ornstein-Uhlenbeck process provides a flexible scheme that can produce distributions of forces in which initial values (F_0), stochasticity (σ), stationary expected values (μ), and rates at which means are obtained (θ), can be variables. This Gaussian process also has the useful property that expected values and variances can be calculated analytically, e.g. [43]. An Ornstein-Uhlenbeck distribution of forces along the river at each time step can be expressed as

$$F_x = F_{x-\delta_x} + \theta\left(\mu - F_{x-\delta_x}\right)\delta_x + \sigma \mathrm{d}W_x. \tag{4.21}$$

The grey curves in Figure 10a show examples of forces calculated in this way for ten time steps. The single black curve is shown to aid visualisation of the variability of a single realisation. In this example, $\theta = 10^{-3}$, $\mu = 5$, and $\sigma = 2 \times 10^{-2}$. The initial force (at the head of the 'river') $F_0 = 1$. The solid and dashed black curves in Figure 3a show expected values and variance where

$$\langle F_x \rangle = \mu + (F_0 - \mu)\exp(-\theta x) \quad \text{and} \quad \mathrm{Var}(F_x) = \frac{\sigma^2}{2\theta}\left[1 - \exp(-2\theta x)\right], \tag{4.22}$$

respectively, see e.g. [43]. Since the Ornstein-Uhlenbeck process produces Gaussian distributions, similar to the normal distributions already examined, the probability of erosion can be calculated analytically. The probability that the erosional force F_x is greater than the critical value for erosion c (e.g. red line in panel a), given F_0, can be expressed as

$$P(F_x > c|F_0) = P(F_x - c > 0|F_0) = 1 - \phi\left(\frac{c - \langle F_x \rangle}{\sqrt{\mathrm{Var}(F_x)}}\right). \tag{4.23}$$

Results of this calculation are shown in Figure 10b. Note that the probability of erosion tends to 1 towards the mouth of the 'river' in this example where $F > c$ at almost all time steps in all realisations. The probability of erosion decreases head-wards, tending to zero where $F < c$.

Expected values and variances of arbitrary distributions of force could of course be estimated numerically by running simulations, such as the one shown in Figure 10c. This panel shows the results of running the linear programme in which the starting solution is simply a linear function that decreases from the head to the mouth of the 'river'. It is evolved according to Equation 4.2. F_x is different at each time step, but is always drawn from the same probability distribution (cf. grey and black curves in panel a). The resultant evolving longitudinal 'river' profile has considerable complexity at small scales (note roughness at small scales). In contrast, evolution at large scales resembles head-ward migration of a kinematic erosional wave. The results at large scales are consistent with calculated expected displacement and its variance estimated using Equation 4.22. It is now straightforward to incorporate estimates of actual body and surface forces driving and resisting erosion in fluvial systems into the stochastic theory.

(iii) Estimating stochastic erosional and resisting forces

Forces in eroding fluvial systems arise from the interaction of flowing water with substrate mass and the geometry of the system. It is straightforward to estimate values in some situations, for example, for the block toppling process explored already in this paper and elsewhere [25,37,45]. Moments (torque) driving erosion in this simple scheme arise from forces associated with drag ($F_d = \rho C_d u^2 h_1/2$), shear along the top of the block ($F_{\tau'} \approx \rho g \Delta z L h_2$), and buoyancy ($F_b = \rho g L h_3$), noting that unit area is assumed. Parameters and typical values are as follows, density of water, $\rho = 1$ Mg/m^3, drag coefficient, C_d, is dimensionless and O(1) [47], u is velocity of water, O($1 - 10$ m/s), h_1, h_2 and h_3 are respective lengths for drag, shear and buoyancy, all typically O($1 - 10$ m) but can be zero (e.g. for no flow). Rarely h_3 can be O(100 m), e.g. Figure 6a. L is the width of the block, substrate density $\rho_r \approx 2 - 3$ Mg/m^3. Thus the forces driving erosion, $F \approx F_d + F_{\tau'} + F_b$, in this simple example are typically O($10^4 - 10^6$ N), but can be as low as zero, see [21] and references therein. The mass of the block provides a body force ($F_g = \rho_r g L H$, H is block height) to resist erosion, which is O($10^4 - 10^5$ N). Torque depends on the width and length of the blocks. For simplicity we assume both are O(1 m). Incorporating other stochastic driving and resisting forces (e.g. friction) into the stochastic approach is straightforward.

Figure 11 shows the results from solving Equation 4.2 in a suite of simulations with stochastic forces driving erosion O($10^4 - 10^5$ N) and constant critical resisting force, $c^* = 10^5$ N. Ten simulations, each with different forcing drawn from the same Ornstein-Uhlenbeck distribution, are used to generate an ensemble of predicted profiles. Figure 11a shows forces at select time steps calculated using Equation 4.21, with $\theta = 5 \times 10^{-3}$ 1/L, $\mu = 2 \times 10^5$ N, $\sigma = 5 \times 10^3$ N/L$^{-1/2}$, and $F_0 = 5 \times 10^4$ N. Expected forces and variance are calculated using Equation 4.22. Probabilities of erosion calculated by solving Equation 4.23 are shown in panel b. The evolution of one simulation is shown in panel c. A zoom into a small portion of this simulation, centred on (190, 250), and another simulation are shown in panels d and e, respectively. The evolution of entire longitudinal profiles is shown for all simulations at five time steps in panel f. These results are shown alongside calculated expected displacement of erosional fronts that originate from the 'mouth' of the river at (1000, 0). Panel g shows profiles from the ten simulations centred on (190, 250) at the same time step (600). These panels demonstrate the complexity and variability of profile geometries possible at small scales when forces driving erosion are stochastic, even when starting conditions are very simple (see e.g. black line in panel f). They also demonstrate that it is possible to generate evolving profiles that naturally incorporate complex geometries at small scales and relatively simple, emergent, geometries at large scales. The evolving geometries, in this example, resemble a 'fuzzy' propagating kinematic wave at large scales (e.g. panel f).

5. Discussion

Pioneering work on stochastic eroding systems has tended to focus on evolution of sedimentary and hydraulic systems, see e.g. [3–11] and references therein. In contrast, at the scale of evolving landscapes, the role of randomness in generating fluvial landforms is poorly understood. Nonetheless, pioneering work by [28,29] demonstrated the important of considering 'quenched noise' in the evolution of fluvial landscapes. We also note that randomness is often incorporated into the starting conditions of many landscape evolution simulators, e.g. Landlab, as a means to enforce channelisation [21,22]. The results from this paper indicate that it is possible to also incorporate stochasticity into a theory of fluvial landscape evolution, in particular in situations where evolution of slopes is important, for instance, along evolving longitudinal river profiles.

We explored three approaches to incorporate stochasticity into a theory of fluvial erosion and landscape evolution. First, incorporating randomness into the velocity of propagating erosion fronts (e.g. waterfalls) was explored the use of equations of Langevin's type. A complimentary approach that uses the Fokker-Planck equation to calculate temporal evolution

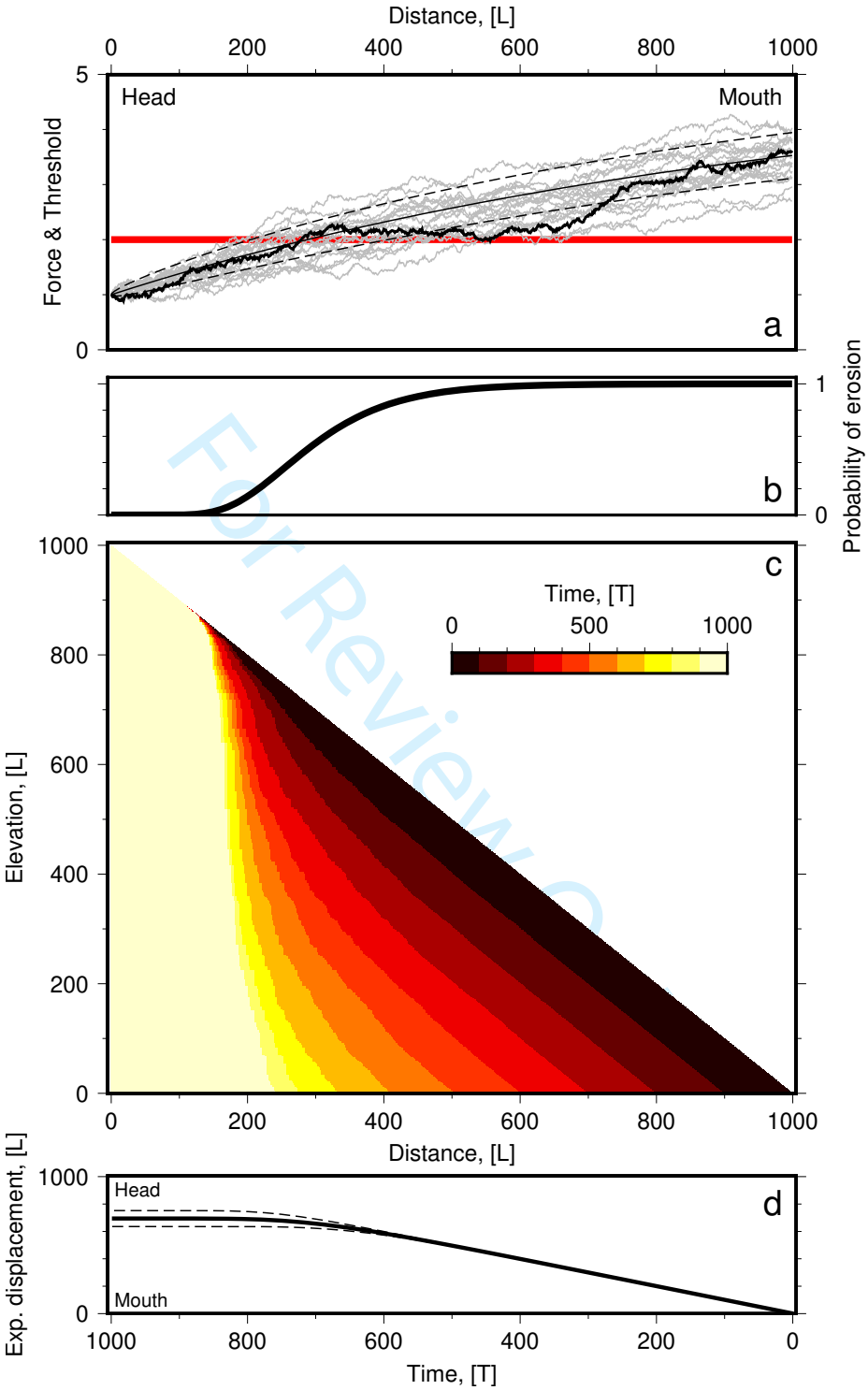

Figure 10. Longitudinal profile evolution with variable probabilities of erosion. In this example, forces driving erosion are calculated using the Ornstein-Uhlenbeck (OU) process. (a) Grey/black curves = forces as a function of distance along a river at ten/single select time steps demonstrating stochasticity. Red line = assumed critical threshold for erosion. Dashed and dotted curves = expected values and variance for the OU process (Equation 4.22). (b) Probabilities of erosion given expected forces, their variance, and critical threshold (Equation 4.23). (c) Longitudinal profile evolution subject to history of forces indicated in panel a, see Equation 4.1. (d) Expected displacement (solid curve) and variance (dashed) of erosional front starting at the mouth of the river (1000, 0; Equation 4.22).

of probability distributions of propagating erosional fronts was examined. Both approaches provide a straightforward way to incorporate stochasticity into landscape evolution problems. They are, however, somewhat removed from the physics associated with erosion and, as parameterised, occasionally predict propagation of erosional fronts downstream. Consequently, we examined methodologies that allow for more arbitrary distributions of forces and critical thresholds of erosion (and proxies, e.g. relief). Analytical approaches for calculating probabilities of erosion, resultant displacement of erosional fronts and associated variance were explored. These approaches tested assumptions of normally and exponentially distributed relief, with calibration of rate parameters using the heights of waterfalls. Finally, a theory for including stochastic erosion in the evolution of longitudinal river profiles was explored. The Ornstein-Uhlenbeck process was found to be a flexible means to parameterise erosional forces. Its Gaussianity enables expected displacements and variance to be calculated analytically, which is useful for testing predictions from the linear programming approach.

The Markovian approaches explored in this paper provide straightforward means to incorporate physics of fluvial erosion into landscape evolution simulations. They include natural emergence of discontinuities and steps that can propagate at different velocities without the need for special numerical treatment. Consequently, many of the challenges associated with developing techniques to predict fluvial landscape evolution using a continuum-based approach, e.g. stability (Courant) conditions, multi-valued functions when shocks develop, are avoided.

The stochastic theory explored has several geomorphic implications. First, it raises the prospect of inferring long term rates of landscape evolution from observations at small scales. For instance, repeat measurements of the forces (or phenomena that dictate forces, e.g. discharge) available for erosion (e.g. over multiple seasons), or erosion rates measured on longer time scales could constrain stochasticity and hence be useful for estimating expected values and variance. However, it raises the obvious problem that identifying long-term trends (e.g. expected displacements) from sparse observations, which could be obtained from, for example, fast, slow or 'mean reverting' trajectories, could be very challenging. We note that the variance of trajectories of erosional fronts calculated in this study tends to increase with age. We also note that variance of erosion can be substantial when critical thresholds for erosion are within the variance of driving forces. The system is simpler when very many observations are available and focus is on large scales.

There are various obvious limitations to what we present that could be addressed in future work. First, we assume that erosional events are independent. They may not be and exploring dependence would be interesting future work. For instance, a slightly more complicated stochastic model could enforce erosion of neighbouring 'blocks' if certain conditions are met. Preliminary results from such a scheme indicates simplicity remains emergent at large scales. Second, we have not incorporated material once it has been eroded. Sedimentary cover could be straightforwardly incorporated, for example, by distributing eroded masses downstream in such a way that conserves mass, perhaps randomly. Third, relatedly, we might consider the incorporation of (stochastic) source terms that could provide means to include, for instance, short wavelength uplift or biota. Finally, generalising this scheme to understand stochastic landscape evolution in two dimensions, e.g. $z(x, y)$, might be fruitful. It would be a step towards developing inverse methodologies to recover information from landscape geometries about processes that govern landscape evolution (e.g. uplift, climate) in the presence of inherently random erosion.

6. Conclusion

Disentangling origins of continental landscapes provides crucial information about geologic, climatic, biotic and geomorphic processes. However, an important complicating problem is that a diverse suite of erosional processes, operating on spatial and temporal scales < 1 to $> 10^7$ meters

royalsocietypublishing.org/journal/rspa Proc R Soc A 0000000

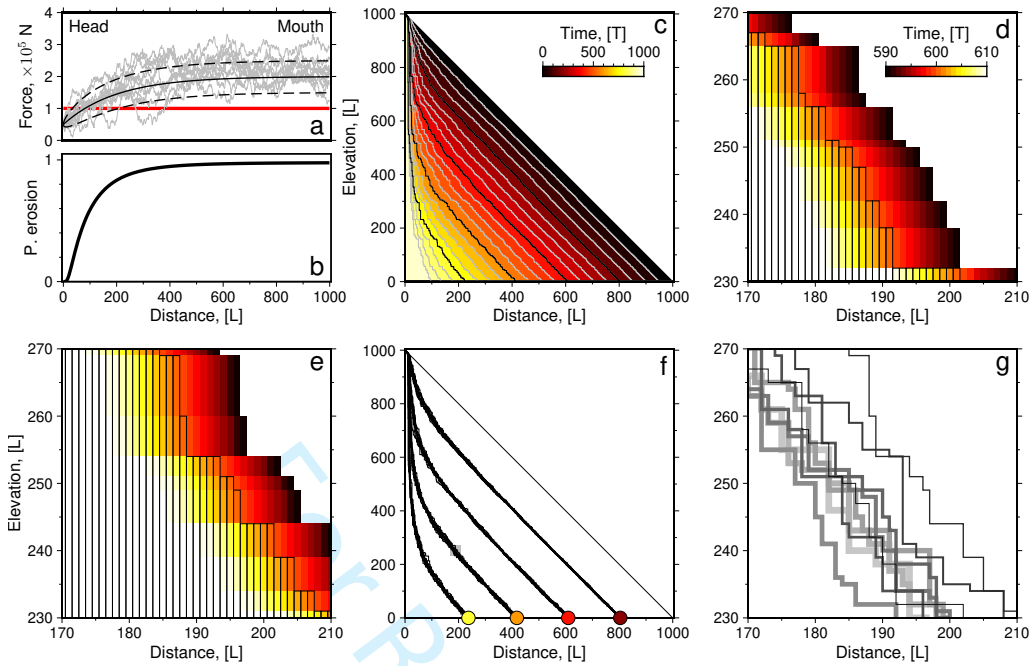

Figure 11. Demonstration of local erosional complexity and emergent simplicity for an evolving theoretical river profile subject to stochastic forcing. (a-b) Examples of inserted forces (grey), associated expected values and variance (solid and dashed), critical threshold (red), and resultant analytical probabilities of erosion (thick black; see Figure 10a-b for extended explanation). (c) Example of profile evolution in one simulation. Grey and black curves = profiles every 50 and 200 time steps, respectively. (d) Zoom into panel c. Black outlined bars = river profile at time step 600. (e) Zoom into a separate simulation that has different random driving forces (but same distribution). Black outlined bars = time step 600. Note differences between evolution and resultant profiles in panels d and e. (f) 'Fuzzy' black curves = profiles at 200, 400, 600 and 800 time steps (e.g. black curves in panel c) from 10 simulations with different random driving forces (but same distribution). Straight line = starting condition. Circles = expected displacements of erosional front originating at the mouth of the 'river' at (1000, 0); colors = time steps (see panel c for scale); calculated variance is smaller than symbol size. Small grey square centred at (190, 250) = position of zoomed-in region shown in panels d, e and g. (g) Calculated positions of longitudinal profiles at time step 600 for the 10 simulations shown in panel f. Colors and line widths simply indicate profiles from different simulations for clarity. Note their variability.

and years, contribute to the evolution of landscapes. As far as we are aware, a theory of fluvial erosion that can self-consistently predict geometries across the scales of interest does not exist. Consequently, we develop a stochastic theory of fluvial erosion that naturally incorporates scale-dependent variability, and the inherent randomness and 'unknowability' of erosional processes. Three approaches are explored. First, stochastic differential equations of Langevin's type and the Fokker-Planck equation are used to incorporate randomness into the motion of erosional fronts (e.g. waterfalls). Second, more flexible analytical schemes incorporating probabilities of erosion calculated using distributions of driving forces and critical thresholds for erosion (and proxies) are explored. Finally, a flexible linear programming approach that can incorporate arbitrary probabilities of erosion into the evolution of theoretical longitudinal river profiles is developed. The Ornstein-Uhlenbeck process is used to parameterise random forcing of erosional processes, which, helpfully, can also be used to develop analytical insight. We demonstrate that the inherent randomness of erosion can generate complex geometries at small scales and emergent simplicity at large scales. It emphasises the importance of considering scale in interpreting observational or theoretical insights into evolution and geometries of landscapes eroded by rivers. We suggest that stochastic theory provides means to understand landscape evolution across the scales of interest.

7. Appendices

[A] The derivation of Equation 4.15 is as follows. First, the probability that $\Delta z > c$ is recast as $P(\Delta z - c > 0) = P(\zeta > 0)$. ζ is then converted into a standard normal distribution (i.e. with mean, $\mu_{\zeta^*} = 0$, and standard deviation, $\sigma_{\zeta^*} = 1$) so that we can later make use of a Standard Normal Cumulative Distribution table. Thus, $\zeta^* = \zeta - \mu_\zeta/\sigma_\zeta$, and $P(\zeta > 0)$ is then shifted to $P(\zeta^* > (0 - \mu_\zeta)/\sigma_\zeta)$, and hence the probability that $\zeta > 0$ becomes

$$P\left(\frac{\zeta - \mu_\zeta}{\sigma_\zeta} > \frac{0 - \mu_\zeta}{\sigma_\zeta}\right), \tag{7.1}$$

which is equivalent to

$$1 - \Phi\left(\frac{0 - \mu_\zeta}{\sigma_\zeta}\right) = P(\zeta > 0) = P(\Delta z > c), \tag{7.2}$$

where Φ is the Normal Cumulative Distribution Function, which yields Equation 4.15 in the main manuscript. In the examples presented in this paper the Python `scipy.stats` library is used to calculate $P(\Delta z > c) = 1 - \texttt{norm.cdf}\{0 - \mu_\zeta/\sigma_\zeta\}$.

[B] In Section v a rate parameter for the exponential distribution of relief along rivers globally is sought using waterfall heights. The challenge with using this dataset to estimate the value of a rate parameter is clear: only large reliefs are included in this dataset. A value is estimated using the Maximum Likelihood Estimator. The probability density function is assumed to be a left-truncated exponential distribution. The derivation of Equation 4.19 in the main text follows. First, consider that the assumed (complete) probability distribution of river reliefs, Δz, is given by $f(\Delta z|\lambda) = \lambda \exp(-\lambda \Delta z)$, for $\Delta z \geq 0$, with support on the interval 0 to ∞. The cumulative density function, $F(\Delta z|\lambda) = 1 - \exp(-\lambda \Delta z)$ for $\Delta z \geq 0$, and zero otherwise. Here we are interesting in using the heights of waterfalls, which have truncated support between τ^* and ∞. The truncated probability distribution can be expressed as

$$f(\Delta z|\lambda, \Delta z > \tau^*) = \frac{\lambda \exp(-\lambda \Delta z)}{1 - F(\tau^*)} I = \lambda \exp[\lambda(\tau^* - \Delta z)] I. \tag{7.3}$$

where $I(\Delta z) = 1$ for $\tau^* < \Delta z < \infty$ and 0 otherwise. The term $1 - F(\tau^*) = \exp(-\lambda \tau^*)$ normalises the truncated probability distribution to ensure that it integrates to (total probability) 1, which is the crucial conceptual step in this derivation. For a single measurement of relief within the truncated support, the maximum likelihood for the value of λ given the available data, can be expressed as $\mathcal{L}(\lambda|\Delta z_1) = \lambda \exp[-\lambda(\tau^* - \Delta z_1]$. With two estimates of relief, $\mathcal{L}(\lambda|\Delta z_1$ and $\Delta z_2) = \mathcal{L}(\lambda|\Delta z_1)\mathcal{L}(\lambda|\Delta z_2) = \lambda \exp[-\lambda(\tau^* - \Delta z_1)] \lambda \exp[-\lambda(\tau^* - \Delta z_2)]$, which can be rearranged to $\lambda^2 \exp[-\lambda[(\tau^* - \Delta z_1) + (\tau^* - \Delta z_2)]$. Thus for n measurements of relief in the truncated series $\mathcal{L}(\lambda|\Delta z_1 \ldots \Delta z_n, \tau^*) = \lambda^n \exp\{-\lambda[(\tau^* - \Delta z_1) + \ldots + (\tau^* - \Delta z_n)]\}$, which can be expressed in the form given by Equation 4.18 in the main manuscript. The derivative of the natural logarithm of this function is given by

$$\frac{\mathrm{d}}{\mathrm{d}\lambda} \ln[\mathcal{L}(\lambda|\Delta z_1 \ldots \Delta z_n, \tau^*)] = \frac{\mathrm{d}}{\mathrm{d}\lambda} \ln\left[\lambda^n \exp\left(\lambda n \tau^* - \lambda \sum_{i=1}^{n} \Delta z_i\right)\right], \tag{7.4}$$

Since $\mathcal{L}(\lambda)$ is expected to be greatest where $\mathrm{d}\mathcal{L}/\mathrm{d}\lambda = 0$, by setting the left-hand side to zero, and solving the derivative on the right-hand side we obtain

$$0 = \frac{n}{\lambda} + n\tau^* - \sum_{i=1}^{n} \Delta z_i, \tag{7.5}$$

which can be rearranged to produce Equation 4.19 in the main manuscript.

Acknowledgements. We thank T Burns and C O'Malley for their help. `gmt` and `matplotlib` libraries are used for plotting. GR thanks M Lamb for supporting a visit to Caltech, and the NERC (NE/T012501/1, NE/X010805/1) for support. OW thanks the Swiss National Science Foundation for supporting with its Early Postdoc Mobility Fellowship (grant number: P2EZP2 195654).

References

1. Anderson RS, Anderson SP. 2010. Geomorphology, The Mechanics and Chemistry of Landscapes. *Cambridge University Press*, ISBN: 9780521519786.
2. Roberts GG, White NJ and Lodhia BH. 2019. Generation and Scaling of Longitudinal River Profiles. *JGR: Earth Surf.*, doi:10.1029/2018JF004796.
3. Einstein, HA. 1950. The bed-load function for sediment transportation in open channel flows, *Tech. Rep. 1026*, U.S. Dept, of Agriculture, Washington, D. C.
4. Fan N, Zhong D, Wu B, Foufoula-Georgiou E, Guala M. 2014. A mechanistic-stochastic formulation of bed load particle motions: From individual particle forces to the Fokker-Planck equation under low transport rates, *JGR: Earth Surf.*, 119, 464–482, doi:10.1002/2013JF002823.
5. Foufoula-Georgiou, E., V. Ganti, and W. E. Dietrich (2010), A nonlocal theory of sediment transport on hillslopes, *JGR*, 115, F00A16, doi:10.1029/2009JF001280.
6. Furbish DJ, Haff PK. 2010. From divots to swales: Hillslope sediment transport across divers length scales, *JGR*, 115, F03001, doi:10.1029/2009JF001576.
7. Furbish, DJ, Roering JJ. 2013. Sediment disentrainment and the concept of local versus nonlocal transport on hillslopes, *JGR: Earth Surf.*, 118, 937–952, doi:10.1002/jgrf.20071.
8. Furbish DJ, Schmeeckle WM. 2013. A probabilistic derivation of the exponential-like distribution of bed load particle velocities, *Water Resour. Res.*, 49, 1537–1551, doi:10.1002/wrcr.20074.
9. Furbish DJ, Haff PK, Roseberry JC, Schmeeckle MW. 2012. A probabilistic description of the bed load sediment flux: 1. Theory, *JGR*, 117, F03031, doi:10.1029/2012JF002352.
10. Parker G, Paola C, Leclair S. 2000. Probabilistic Exner sediment continuity equation for mixtures with no active layer, *J. Hydraul. Eng.*, 126, 818–826.
11. Ancey C, Bohorquez P, Heyman J. 2015. Stochastic interpretation of the advection-diffusion equation and its relevance to bed load transport. *JGR: Earth Surf.* **120**, doi:10.1002/2014JF003421.
12. Farley KA. 2002. (U-Th)/He dating: Techniques, calibrations, and applications. *Rev. in Min. and Geochem.*, 47(1), 819–844.
13. Flowers RM, Farley KA. 2012. Apatite 4He/3He and (U-Th)/He evidence for an ancient Grand Canyon. *Science*, 338, 1616–1619, doi:10.1126/science.1229390.
14. Galloway WE. 2001. Cenozoic evolution of sediment accumulation in deltaic and shore-zone depositional systems, Northern Gulf of Mexico Basin. *Marine and Pet. Geol.*, 18(10), 1031–1040. doi:10.1016/S0264-8172(01)00045-9.
15. Czarnota K, Roberts GG, White NJ, Fishwick S. 2014. Spatial and temporal patterns of Australian dynamic topography from river profile modeling. *JGR: Solid Earth*, 119, 1384–1424. doi:10.1002/2013JB010436.
16. Wellman P, McDougall I. 1974. Potassium-argon ages on the Cainozoic volcanic rocks of New South Wales, *J. Geol. Soc. Aust.*, 21(3), 247–272, doi:10.1080/00167617408728849.
17. Rosenbloom NA, Anderson RS. 1994. Hillslope and channel evolution in a marine terraced landscape, Santa Cruz, California, *JGR*, 99(B7), 14,013–14,029, doi:10.1029/94JB00048.
18. Stock JD, Montgomery DR. 1999. Geologic constraints on bedrock river incision using the stream power law, *JGR*, 104(B3), 4983–4993, doi:10.1029/98JB02139.
19. Howard AD, Dietrich WE, Seidl MA. 1994. Modeling fluvial erosion on regional to continental scales, *JGR*, 99(B7), 13,971–13,986, doi:10.1029/94JB00744.
20. Whipple KX, Tucker GE. 1999. Dynamics of the stream-power river incision model: Implications for height limits of mountain ranges, landscape response timescales, and research needs, *JGR*, 104(B8), 17,661–17,674, doi:10.1029/1999JB900120.
21. Lague D. 2014. The stream power river incision model: Evidence, theory and beyond. *Earth Surf. Proc. and Landforms*, 39, 38–61. doi: 10.1002/esp.3462.
22. Hobley DEJ, Adams JM, Nudurupati SS, Hutton EWH, Gasparini NM, Istanbulluoglu E, Tucker GE. (2017). Creative computing with Landlab: An open-source toolkit for building, coupling, and exploring two-dimensional numerical models of Earth-surface dynamics. *Earth Surf. Dyn.*, 5, 21–46. doi: 10.5194/esurf-5-21-2017.
23. Salles T. 2016. Badlands: A parallel basin and landscape dynamics model. *SoftwareX*, 5, 195–202. doi:10.1016/j. softx.2016.08.005.
24. Roberts GG, White N. 2010. Estimating uplift rate histories from river profiles using African examples. *JGR*, 115, B02406. doi:10.1029/2009JB006692.

25. Lamb MP, Dietrich WE. 2009. The persistence of waterfalls in fractured rock: *Geol. Soc. Am. Bull.*, 121, 1123–1134, doi:10.1130/B26482.1.
26. Ferdowsi B, Ortiz CP, Jerolmack DJ. 2018. Glassy dynamics of landscape evolution. *PNAS*. 115(9), 4827–4832.
27. Roberts GG, White N, Lodhia BH. 2019. The generation and scaling of longitudinal river profiles. *JGR*, 124, 137–153, doi:10.1029/2018JF004796.
28. Wapenhans I, Fernandes V, O'Malley C, White NJ and Roberts GG. 2021. Scale-Dependent Contributors to River Profile Geometry, *JGR: Earth Surf.*, doi:10/1029/2020JF005879.
29. Smith TR, Bretherton FP. 1972. Stability and the conservation of mass in drainage basin evolution. *Wat. Res. Res.*, 8, 1506–1529, doi:10.1029/WR008i006p01506.
30. Birnir B, Smith TR, Merchant GE. 2001, The scaling of fluvial landscapes: *Comp. & Geosci.*, 27, 1189–1216, doi:10.1016/S0098-3004(01)00022-X.
31. Sklar L, Dietrich WE. 1998. River longitudinal profiles and bedrock incision models: Stream power and the influence of sediment supply, in Tinkler, K.J., and Wohl, E.E., eds., Rivers Over Rock: Fluvial Processes in Bedrock Channels: AGU Geophys. Mono. 107, 237–260, doi:10.1029/GM107p0237.
32. Bursztyn N, Pederson JL, Tressler C, Mackley RD, Mitchell KJ. 2015. Rock strength along a fluvial transect of the Colorado Plateau: Quantifying a fundamental control on geomorphology. *EPSL*, 429, 90–100. doi:10.1016/j.epsl.2015.07.042.
33. Molnar P. 2004. Interactions among topographically induced elastic stress, static fatigue, and valley incision. *JGR: Earth Surf.*, 109, F02010, doi:10.1029/2003JF000097.
34. Glotzbach C. 2015. Deriving rock uplift histories from data-driven inversion of river profiles. *Geology*, 43, 467–470. doi:10.1130/G36702.1.
35. Goren L, Fox M, Willett SD. 2014. Tectonics from fluvial topography using formal linear inversion: Theory and applications to the Inyo Mountains, California. *JGR: Earth Surf.*, 119, 1651–1681. doi:10.1002/2014JF003079.
36. Fernandes VM, Roberts GG, White N, Whittaker AC. 2019. Continental-scale landscape evolution: A history of North American topography. *JGR: Earth Surf.*, 124, 2689–2722. doi:10.1029/2018JF004979.
37. Stucky de Quay G, Roberts GG, Rood DH, Fernandes VM. 2019. Holocene uplift and rapid fluvial erosion of Iceland: A record of post-glacial landscape evolution. *EPSL*, 505, 118–130, doi:10.1016/j.epsl.2018.10.026.
38. Zondervan JR, Whittaker AC, Bell RE, Watkins SE, Brooke SAS, Hann MG. 2020. New constraints on bedrock erodibility and landscape response times upstream of an active fault. *Geomorph.*, 351, 106937. doi:10.1016/j.geomorph.2019.106937.
39. O'Malley CPB, White NJ, Stephenson SN, Roberts GG. 2021. Large-Scale Tectonic Forcing of the African Landscape. *JGR: Earth Surf.*, 126, e2021JF006345. doi:10.1029/2021JF006345.
40. Roberts GG. 2019. Scales of similarity and disparity between drainage networks. *GRL*, 46, 3781–3790. doi:0.1029/2019GL082446.
41. Pritchard D, Roberts GG, White N, Richardson C. 2009. Uplift histories from river profiles. *GRL*, 36, L24301, doi:10.1029/2009GL040928.
42. Royden L, Perron JT. 2013. Solutions of the stream power equation and application to the evolution of river longitudinal profiles. *JGR: Earth Surf.*, 118(2), 497–518. doi:10.1002/jgrf.20031.
43. Gardiner CW. 2004. Handbook of Stochastic Methods for Physics, Chemistry and the Natural Sciences. *Springer Series in Synergetics*, **13**.
44. Risken H. 1992. The Fokker-Planck Equation, Methods of Solution and Applications. *Springer Series in Synergetics*.
45. Roberts GG. 2021. Emergent simplicity despite local complexity in eroding fluvial landscapes. *Geology* **49**(11), doi:10.1130/G48942.1.
46. Farr TG et al. 2007. The Shuttle Radar Topography Mission, *Rev. Geophys.*, 45, RG2004, doi:10.1029/2005RG000183.
47. Batchelor G. 1967. An Introduction to Fluid Dynamics. *Cambridge University Press*.